

UNIVERSITY OF SOUTHAMPTON

**Disc Winds Matter: Modelling
Accretion and Outflow on All Scales**

by

James Matthews

A thesis submitted in partial fulfillment for the
degree of Doctor of Philosophy

in the
Faculty of Physical Sciences and Engineering
Department of Physics & Astronomy

March 2016

UNIVERSITY OF SOUTHAMPTON

Abstract

Faculty of Physical Sciences and Engineering

Department of Physics & Astronomy

Doctor of Philosophy

by James Matthews

The Thesis Abstract is written here (and usually kept to just this page). The page is kept centered vertically so can expand into the blank space above the title too...

Contents

Abstract

i

1	Introduction	1
1.1	The Physics of Accretion	3
1.1.1	Spherical Accretion and The Eddington Limit	4
1.1.2	Accretion Discs	5
1.1.2.1	Steady-state Accretion Discs: The α -prescription	6
1.1.3	Boundary layers, black hole spin and the ISCO	7
1.1.4	The emergent spectrum	9
1.2	Accreting Compact Binaries	11
1.2.1	Roche Lobe-Overflow	13
1.2.2	Cataclysmic Variables	14
1.2.2.1	Dwarf Novae and the Disc-instability Model	15
1.2.2.2	Nova-like Variables	15
1.2.3	Low Mass X-ray Binaries	16
1.3	Quasars and Active Galactic Nuclei	19
1.3.1	AGN Unification and the dusty Torus	21
1.3.2	X-ray Properties of AGN	24
1.3.2.1	The Soft X-ray Excess	25
1.3.3	The Broad Line Region: Connection to winds and unification	26
1.4	The Current Understanding of the Disc Continuum	26
1.4.1	The Spectral shape of CV discs	26
1.4.2	The Big Blue Bump in AGN	28
1.4.2.1	The Accretion Disc Size Problem	28
1.4.2.2	Fitting AGN Spectra and the 1000Å Break	28
1.5	The Universality of Accretion	29
1.5.1	The RMS-flux relation	29
1.5.2	Accretion states and disc-jet coupling	30
1.5.3	A Global Picture	31
2	Accretion Disc Winds	32
2.1	Observational Evidence	32
2.1.1	Cataclysmic Variables	33
2.1.2	X-ray Binaries	35
2.1.3	AGN and Quasars	36
2.1.3.1	Broad Absorption Line Quasars	36

2.1.3.2	Warm Absorbers	38
2.1.3.3	Ultra-fast Outflows	38
2.1.4	Stellar Winds	39
2.1.4.1	Clumping	39
2.2	Driving Mechanisms	39
2.2.1	Thermal Winds	41
2.2.2	Radiatively Driven Winds	42
2.2.3	Line-driven Winds	42
2.2.4	Magnetic Winds	42
2.3	Accretion Disc Wind Models	42
2.4	A Kinematic Prescription	42
2.5	The really, really big picture: AGN Feedback	42
2.5.1	Observational evidence for feedback	43
2.5.2	Radiative or quasar mode feedback	43
2.5.3	Kinetic or radio mode feedback	43
2.5.4	Alternative Explanations	43
3	Quasar Emission Line Equivalent Widths as Probes of Orientation and Unification	45
3.1	Data Sample	45
3.2	The Angular Distribution of Emission from an Accretion Disc and Broad-Line Region	48
3.2.1	Standard Thin Disc Models	48
3.2.2	Including GR, Comptonisation and Opacity Effects	49
3.2.3	Alternative Continuum Models: Irradiation and Truncated Discs .	49
3.3	Predicted EW distributions compared to observations: A Monte Carlo approach	49
3.4	Discussion	53
3.4.1	Radio Observations	53
3.4.2	Polarisation	53
3.4.3	Compton-thick Fractions	53
3.4.4	Theoretical Considerations	53
3.5	Conclusions	53
Bibliography		56

Chapter 1

Introduction

“And now you’re asking, I don’t know where to begin”

Mike Vennart, Silent/Transparent

The release of gravitational potential energy as mass falls towards a compact object is the most efficient energetic process in the universe, even more efficient than nuclear fusion. This *accretion* process is thought to power the huge radiative engines at the centres of every galaxy – accreting supermassive black holes known as active galactic nuclei (AGN). As the matter falls into the potential well of the black hole it often forms an accretion disc, which, in many cases, is an efficient radiator of the gravitational energy released. In some cases, the accretion disc can outshine the entire stellar population of the galaxy, appearing as a quasi-stellar object (QSOS) or *quasar*. As well as powering, AGN, accretion discs are present in X-ray binaries (XRBs), young-stellar objects (YSOs) and cataclysmic variables (CVs). Accretion is a universal process; broadly speaking, the physics is similar regardless of whether matter is falling on to a $\sim 1 M_\odot$ Neutron Star or White Dwarf system, or a $\sim 10^{10} M_\odot$ black hole.

Outflows are ubiquitous in accreting systems. We see collimated radio jets in AGN (Hazard et al. 1963; Potash & Wardle 1980; Perley et al. 1984; Marscher 2006) and XRBs (Belloni 2010), and there is even evidence of extended radio emission in CVs (Benz et al. 1983; Coppejans et al. 2015). These radio jets tend to appear in specific accretion states (Fender 2001; Fender et al. 2004; Körding et al. 2008), implying an intrinsic connection to the accretion process. Even more intriguing, in XRBs less collimated, mass-loaded

outflows or *winds* are observed in the opposite accretion state, possibly emanating from the accretion disc. Evidence for disc winds is widespread across the mass range, but perhaps the most spectacular indication is the blue-shifted, broad absorption lines (BALs) in the rest-frame ultraviolet (UV) seen in high-state CVs (Heap et al. 1978; Greenstein & Oke 1982; Cordova & Mason 1982) and the so-called broad absorption line quasars (BALQSOs) that make up 20–40% of quasars (Weymann et al. 1991; Knigge et al. 2008; Allen et al. 2011). BALs and ‘P-Cygni’ profiles (Struve 1935; Rottenberg 1952) are also seen in stellar winds (e.g. Cassinelli 1979) and sometimes even in the optical spectra of CVs (Patterson et al. 1996; Ringwald & Naylor 1998; Kafka & Honeycutt 2004). Broad, blue-shifted absorption is even observed in the Fe K α line in AGN (Reeves et al. 2003; Pounds & Reeves 2009; Tombesi et al. 2010) – these are known as ultra-fast outflows or UFOs.

The astrophysical significance of disc winds extends, quite literally, far beyond the accretion environment. They offer a potential mechanism by which the central accretion engine can interact with the host galaxy and interstellar medium via a ‘feedback’ mechanism (King 2003; Fabian 2012). Feedback is required in models of galaxy evolution (Springel et al. 2005) and may explain the famous ‘ $M - \sigma$ ’ relation (Silk & Rees 1998; Häring & Rix 2004). Winds also offer a natural way to *unify* much of the diverse phenomenology of AGN, CVs and XRBs. The principle of unification can be applied along more than one ‘axis’ of parameter space. For example, there exist elegant models that attempt to explain *all* of the behaviour of quasars with only a central black hole, a jet, an accretion disc, and an associated outflow, by varying the viewing angle (Elvis 2000). Similarly elegantly, it has been shown that much of the behaviour of XRBs is directly applicable to AGN (McHardy et al. 2006), and models of outflows in CVs have been successfully ‘scaled-up’ and applied to quasars and AGN (e.g. Higginbottom et al. 2013).

Despite their clear importance and ubiquity, there are still many unanswered questions relating to the true impact of winds and their underlying physical origins. Here, I aim to address some of these questions, and take steps towards building a more holistic picture of the impact of winds on the spectral appearance and accretion physics of disc systems. This thesis is structured as follows. In the remainder of this chapter, I will give the background accretion theory and detail the successes and failures of accretion disc models when compared to observations, as well as describing the different classes of accreting objects in more detail. In chapter 2, I dedicate some time to specifically

discussing the theory of, and observational evidence for, accretion disc winds. In chapter 3, I outline the Monte Carlo radiative transfer (MCRT) and photoionization methods I have used in order to investigate the impact of disc winds on the spectra of accreting systems. The science chapters contain three separate submitted papers, in which we investigated the impact of disc winds on the spectra of CVs (Chapter 5), and tested disc wind quasar unification models (Chapters 6 and 7). In chapter 8, I summarise my findings and their astrophysical significance, and discuss potential avenues for future work.

1.1 The Physics of Accretion

The basic phenomenon of accretion- matter falling into a gravitational potential well- is a ubiquitous one in astrophysics. The energy, ΔE , released by a parcel of mass Δm falling from infinity onto an object of mass M and radius R_* is given by

$$\Delta E = \frac{GM\Delta m}{R_*}, \quad (1.1)$$

meaning that the accretion power can then be given by

$$L_{acc} = \frac{GM\dot{M}}{R}. \quad (1.2)$$

We can also parameterise any energetic process with the form

$$\Delta E = \eta \dot{M} c^2, \quad (1.3)$$

where η is the radiative efficiency. Nuclear fusion is one of the more efficient energetic processes in the universe, with an efficiency of $\eta = 0.007$. If we rearrange the above equations in terms of η we find

$$\eta = \frac{G}{c^2} \frac{M}{R_*}. \quad (1.4)$$

In other words, the efficiency of accretion is directly related to the *compactness* of the central object.

1.1.1 Spherical Accretion and The Eddington Limit

The simplest geometry one might propose for accretion would be one in which a central mass accretes matter from an all-encompassing cloud or the inter-stellar medium. The process of spherical accretion has come to be known as Bondi-Hoyle-Lyttleton accretion ([Hoyle & Lyttleton 1939](#); [Bondi & Hoyle 1944](#)). In particular, [Bondi \(1952\)](#) studied spherically symmetric accretion onto a point mass and derived the Bondi radius,

$$r_B = \frac{GM}{c_S^2}, \quad (1.5)$$

where $c_S = c_S(r_B)$ is the sound speed as a function of radius. The Bondi radius represents a critical point inside which the material is supersonic and will accrete on the free-fall timescale.

When this timescale is long enough, then the accreting matter can radiate its potential energy with luminosity L . This radiation will induce a force on electrons, given by

$$F_{rad} = \frac{L\sigma_T}{4\pi r^2 c}, \quad (1.6)$$

where $\sigma_T = 6.65 \times 10^{-25} \text{ cm}^2$ is the Thomson cross-section. If this radiation force term dominates over the gravitational force then the material will no longer fall inwards. Consider radiation pressure acting on electron-proton pairs, for which the gravitational force is approximately given by GMm_p/r^2 . Combining this expression with equation 1.6 gives a natural maximum accretion luminosity, known as the *Eddington limit*, of

$$L_{Edd} = \frac{4\pi GMm_p c}{\sigma_T}, \quad (1.7)$$

with an associated Eddington accretion rate of

$$\dot{M}_{Edd} = \frac{L_{Edd}}{\eta c^2}. \quad (1.8)$$

The Eddington limit makes a number of assumptions, namely that the accretion flow is steady, spherically symmetric, ionized, and has its opacities dominated by electron scattering. Clearly, there are many astrophysical situations where this does not hold. For example, the recent outburst of V404 Cyg showed wildly variable luminosities on short timescales (see, e.g., [Kuulkers et al. 2015](#); [Motta et al. 2015](#), among many, many

ATels), and in any binary system or disc dominated system then the assumption of spherical symmetry will break down. Nevertheless, the Eddington limit gives a good order of magnitude estimate of the maximum luminosity of an accreting object, and also provides a useful way of parameterising accretion rate, as it scales linearly with mass. It can also be used to characterise the *state* of an accretion disc. In general, sources around $0.1 L_{Edd}$ find themselves in a soft or thin-disc state , whereas for much lower Eddington fractions sources will form advection dominated accretion flows (ADAFs; [Narayan & Yi 1994, 1995](#)). It is also clear that around the Eddington limit radiation pressure must play a major role in determining the disc morphology (see section [2.2.2](#)).

1.1.2 Accretion Discs

In many astrophysical situations – for example, binary orbits and gas clouds orbiting BHs – any accreting matter will possess some net angular momentum. If the medium is dense enough, then collisions between particles will be frequent, and the total angular momentum vector of two colliding particles will always be conserved. This allows a mechanism for a gas cloud to relax to its minimum energy state – an accretion disc.

As well as losing gravitational potential energy as it falls towards the central mass, a parcel of matter must always lose this angular momentum. Crucially, accretion discs provide a way for a given parcel of mass to lose angular momentum. If the disc itself maintains the same total angular momentum, then it follows that angular momentum must therefore be transported outwards. The mechanism for transporting angular momentum outwards is unknown, and is one of the biggest weaknesses of current accretion disc theory. The most commonly invoked candidate is the magnetorotational instability (MRI; [Balbus & Hawley 1991](#)), in which accretion discs are subject to a strong shearing instability even when the magnetic field is weak. An alternative is that the angular momentum is lost via a a magnetohydrodynamic outflow ([Blandford & Payne 1982](#)). An efficient mechanism for angular momentum transportat is necessary as the viscosity introduced in the next section is generally inefficient in this regard (?).

1.1.2.1 Steady-state Accretion Discs: The α -prescription

The so-called α -disc model developed by ([Shakura & Sunyaev 1973](#), hereafter SS73) and [Lynden-Bell \(1969\)](#) is currently the leading candidate for explaining how energy and angular momentum is transported an accretion disc. The starting point for this model is the parameterisation of viscosity using a simple form of

$$\nu = \alpha c_s H. \quad (1.9)$$

Viscous torques then allow the conversion of orbital kinetic energy into heat, which can be radiated away. If we then make one further assumption, that the accretion rate is constant throughout the disc, then we can write down a mass continuity equation valid at all radii, given by

$$\dot{M} \equiv 2\pi R V_R \Sigma = 0 \quad (1.10)$$

where Σ is the surface density at that point. The angular momentum equation becomes, in this case

$$\nu' \Sigma = \frac{\dot{M}}{3\pi} \left[1 - \left(\frac{R}{R_*} \right)^{1/2} \right] \quad (1.11)$$

The viscous torques throughout the disc cause a local loss of mechanical energy, allowing one to derive (see, e.g. [Frank et al. 1992](#)) a rate of viscous dissipation, per unit area, given by

$$D(R) = \frac{1}{2} \nu' \Sigma (R \Omega')^2. \quad (1.12)$$

Here, $D(R)$ is proportional to the derivative of the angular velocity, $\Omega' = d\Omega/dR$. By combining equations 1.12 and 1.11 we can show that the viscous dissipation rate is

$$D(R) = \frac{GM\dot{M}}{8\pi R^3} \left[1 - \left(\frac{R}{R_*} \right)^{1/2} \right] \quad (1.13)$$

where we have also set the angular velocity to the Keplerian velocity. This expression is, importantly, independent of viscosity – which is fortunate, because we do not know what value of α to use in equation 1.9. This result comes about because of the implicit assumption that the viscosity regulates the mass accretion rate so as to achieve a steady state.

We can now integrate across the whole disc to obtain the disc luminosity,

$$L_{disc} = 2 \int_{R_*}^{\infty} D(R) 2\pi R dR = \frac{GM\dot{M}}{2R_*} = \frac{1}{2} L_{acc}. \quad (1.14)$$

This result can also be shown by considering the binding energy of gas at R_* and infinity. From equation 1.13 one can also derive an effective temperature distribution, by setting

$$\sigma T_{eff}^4(R) = D(R), \quad (1.15)$$

which then gives

$$T_{eff}(R) = T_* \left[1 - \left(\frac{R}{R_*} \right)^{1/2} \right]^{1/4}, \quad (1.16)$$

where

$$T_* = \left(\frac{3GMM}{8\pi R_*^3 \sigma} \right)^{1/4}. \quad (1.17)$$

When $R \gg R_*$ then we can simplify this to

$$T_{eff}(R) = T_* (R/R_*)^{-3/4}. \quad (1.18)$$

Now we have not only derived the total luminosity of an accretion disc, but also the effective temperature profile which will govern the shape of the emergent SED. This temperature profile is shown in figure 1.1 for three different compact objects, assuming an Eddington fraction of 0.2.

1.1.3 Boundary layers, black hole spin and the ISCO

In equation 1.14 I showed that $L_{disc} = 1/2 L_{acc}$. One might then ask: where does the rest of the luminosity go? The answer is dependent on the compact object in question. In an accreting WD, the rotating matter must eventually deposit itself on the surface of the WD. This is illustrated in figure 1.2, which shows the angular velocity as a function of radius in a disc around a compact object rotating with angular velocity Ω_* . The boundary layer (BL) is the region to the left of the dotted line, inside the maximum of Ω_K , the Keplerian angular velocity. The luminosity of the boundary layer is (Frank et al. 1992)

$$L_{BL} = \frac{1}{2} \frac{GM\dot{M}}{R} \left[1 - \left(\frac{\Omega_*}{\Omega_K(R_*)} \right) \right]^2, \quad (1.19)$$

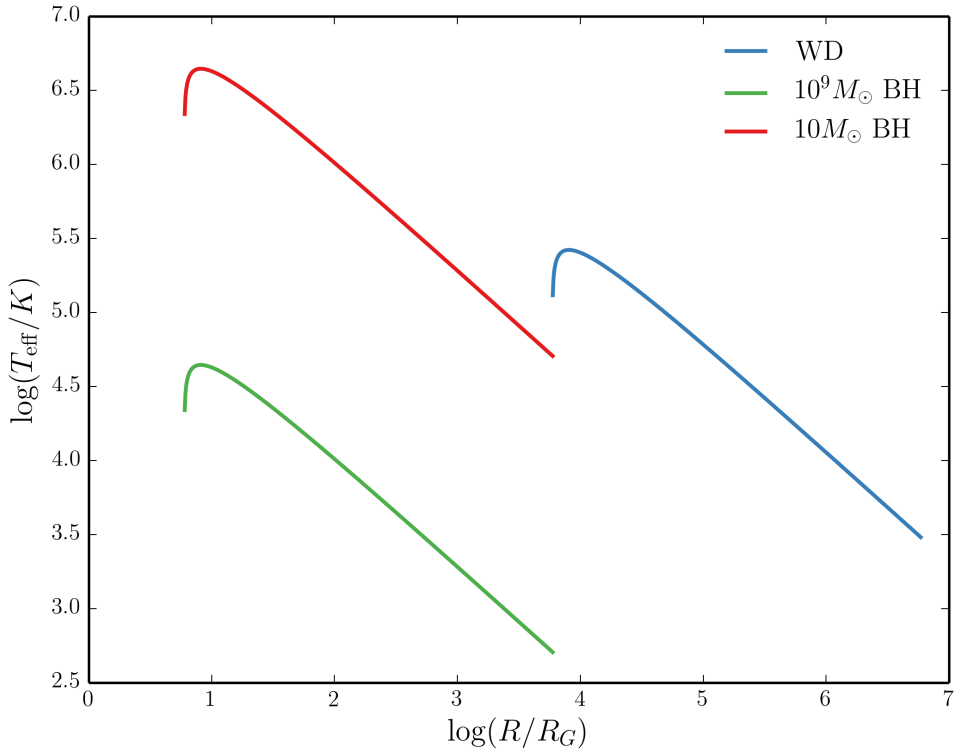


FIGURE 1.1: The temperature profile of an accretion disc for three different classes of compact object.

where $\Omega_K(R_*)$ is the Keplerian angular velocity at R_* , assuming the thickness of the BL is small. When $\Omega_K(R_*) \gg \Omega_*$ this reduces to $L_{BL} = 1/2 L_{acc} = L_{disc}$

BLs can be approximated with blackbodies and their temperatures estimated indirectly via the [Zanstra \(1929\)](#) method (e.g. [Hoare & Drew 1991, 1993](#)), but they likely exhibit a variety of atomic features ([Suleimanov et al. 2014](#)). Extreme-UV datasets have confirmed the existence of boundary layer emission in non-magnetic CVs ([Mauche 1996](#)), although these observations are limited in number.

Clearly, in BH systems a boundary layer cannot exist in the same way, due to the lack of a physical surface, and the energy must either go into growing the BH, contributing to its angular momentum or being channeled into a jet or other radiative source (see section 1.5.2) The question of what happens at the inner disc edge is complicated further by the fact that the disc cannot extend to the event horizon of the BH. Instead, there is an ‘innermost stable circular orbit’ (ISCO) beyond which the accreting matter will simply fall into the BH. The radius of this orbit, R_{ISCO} , and the horizon radius, R_H , is shown for different values of the BH spin parameter, a_* , in figure 1.3, showing how

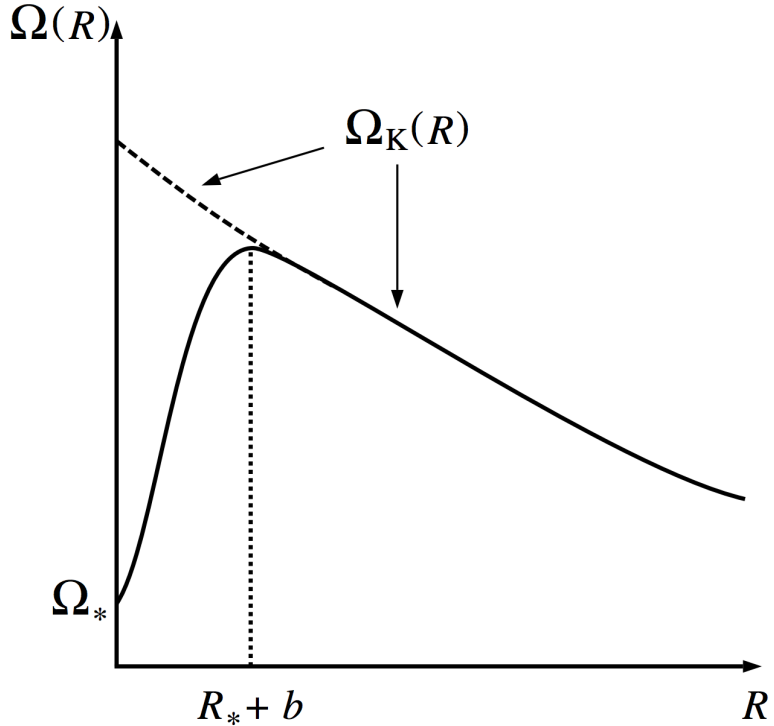


FIGURE 1.2: Credit: Frank et al. 2002. Angular velocity as a function of radius in an accretion disc around a rotating compact object with angular velocity Ω_* . Ω_K is the Keplerian angular velocity. This graph also helps explain why there is a turnover in the temperature-radius relation, as $D(R)$ is proportional to the square of the derivative of this quantity.

matter can orbit closer to a prograde spinning BH. One should really set $R_* = R_{ISCO}$ in equation 1.4, giving us the interesting result that rapidly spinning BHs are more radiatively efficient than Schwarzschild BHs.

1.1.4 The emergent spectrum

It is important to recognise that the steady-state disc treatment *does not specify the exact shape of the disc SED*. What it does do is say where energy is originally released. If one makes the simplest assumption, that each annulus emits as a blackbody with temperature $T_{eff}(R)$ then it is possible to show that at intermediate radii, where $kT(R_{max}) \ll h\nu \ll kT_*$, then the spectrum has the form

$$F_\nu \propto \nu^{1/3} \quad (1.20)$$

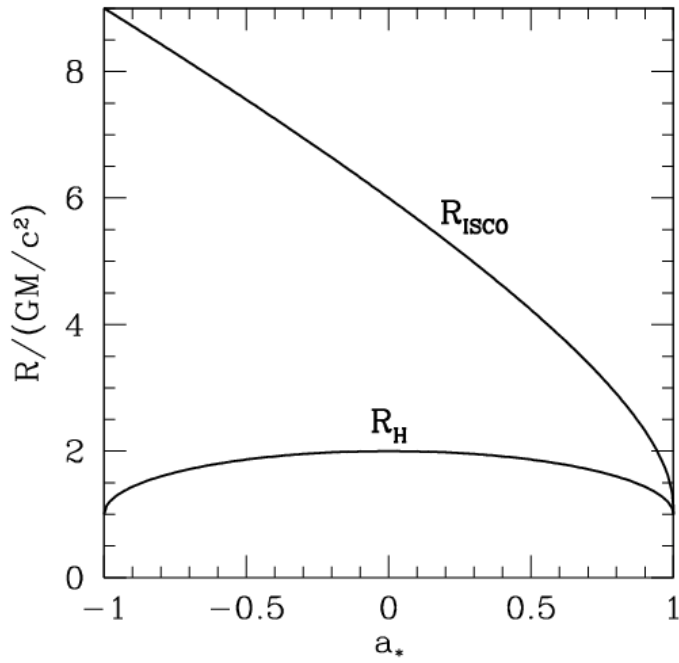


FIGURE 1.3: Credit: Narayan 2014. The radius of the ISCO, R_{ISCO} , and the horizon, R_H , is as a function of the BH spin parameter, a_* . $a_* = 0$ corresponds to a Schwarzschild BH, and $a_* = 1$ and $a_* = -1$ to prograde and retrograde Kerr BHs respectively. Note that this figure ignores the counteracting torque of photons swallowed by the BH, which actually limits a_* to a value of around 0.998 (Thorne 1974).

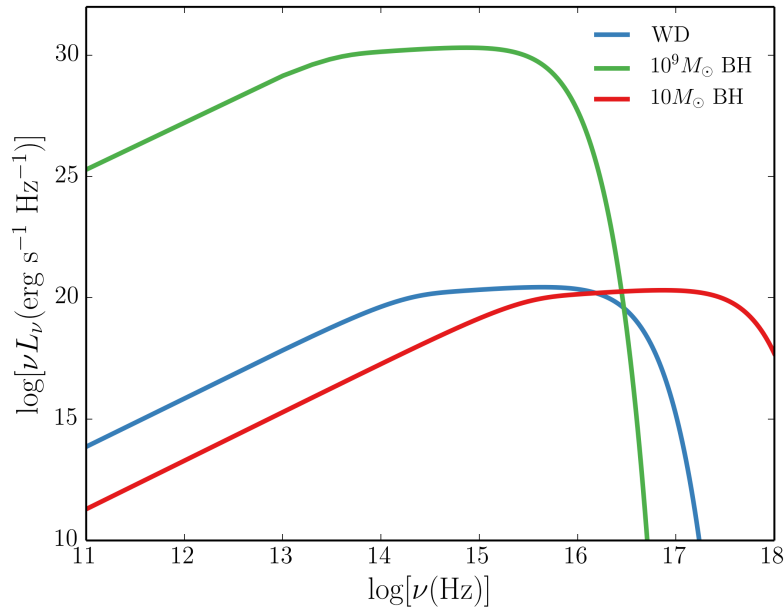


FIGURE 1.4: Accretion disc SEDs for three different compact objects, corresponding roughly to a quasar, an XRB and a CV. The SEDs are computed via an area-weighted sum of blackbodies with effective temperatures governed by equation 1.16, and the $\nu^{1/3}$ shape in the middle of the spectra can be seen.

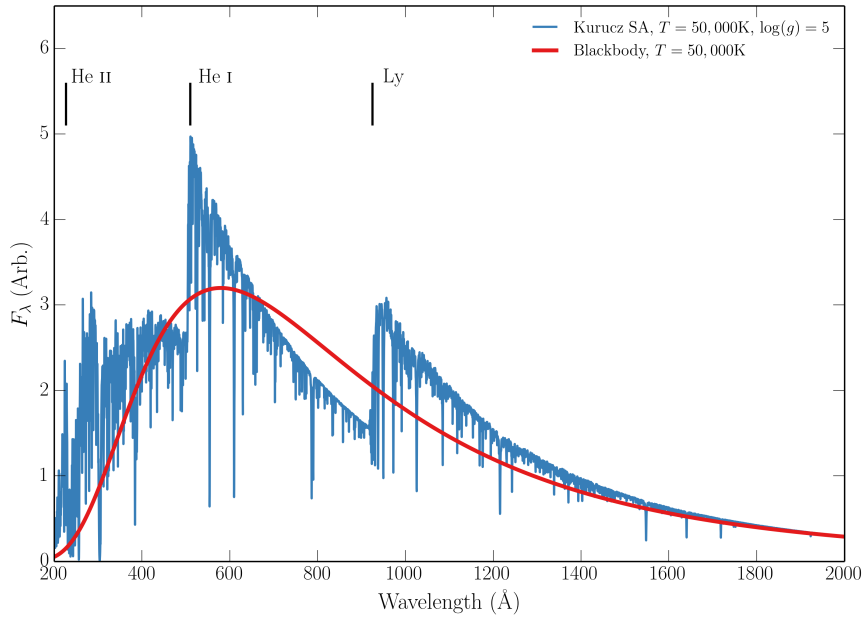


FIGURE 1.5: A comparison between a Planck curve and Kurucz (1991) stellar atmosphere model at $T_{\text{eff}} = 50,000\text{K}$ and surface gravity of $\log(g) = 5$. The major photoabsorption edges are marked. Flux is reprocessed into different wavelengths by bound-free opacities, and line blanketing also has a big effect on the spectrum. The Hydrogen and Helium lines also experience significant pressure broadening.

Figure 1.4 shows the blackbody SEDs expected for the same objects as figure 1.1, in which the $\nu^{1/3}$ law can be clearly seen. A disc atmosphere model with frequency-dependent opacity creates a somewhat different (and more realistic) spectrum. Figure 1.5 shows a comparison between a stellar atmosphere model and blackbody model for $T_{\text{eff}} = 50,000\text{K}$, showing how an annulus at that temperature can have a significantly different spectral shape when one includes frequency-dependent opacities in the atmosphere. It is of course possible that *neither* blackbody or disc atmosphere treatments are realistic. I shall therefore devote a little time to discussing the observational arguments for accretion discs and the different classes of accreting objects.

1.2 Accreting Compact Binaries

Accreting compact binaries form many different classes, but are all characterised by matter streaming from a donor star or secondary onto a compact object or primary. There are only two ways by which matter can transfer from the secondary to the compact object. One is by Roche Lobe-overflow (RLOF), whereby stellar evolution causes the donor star to fill its Roche Lobe, the surface of equipotential around the star. The

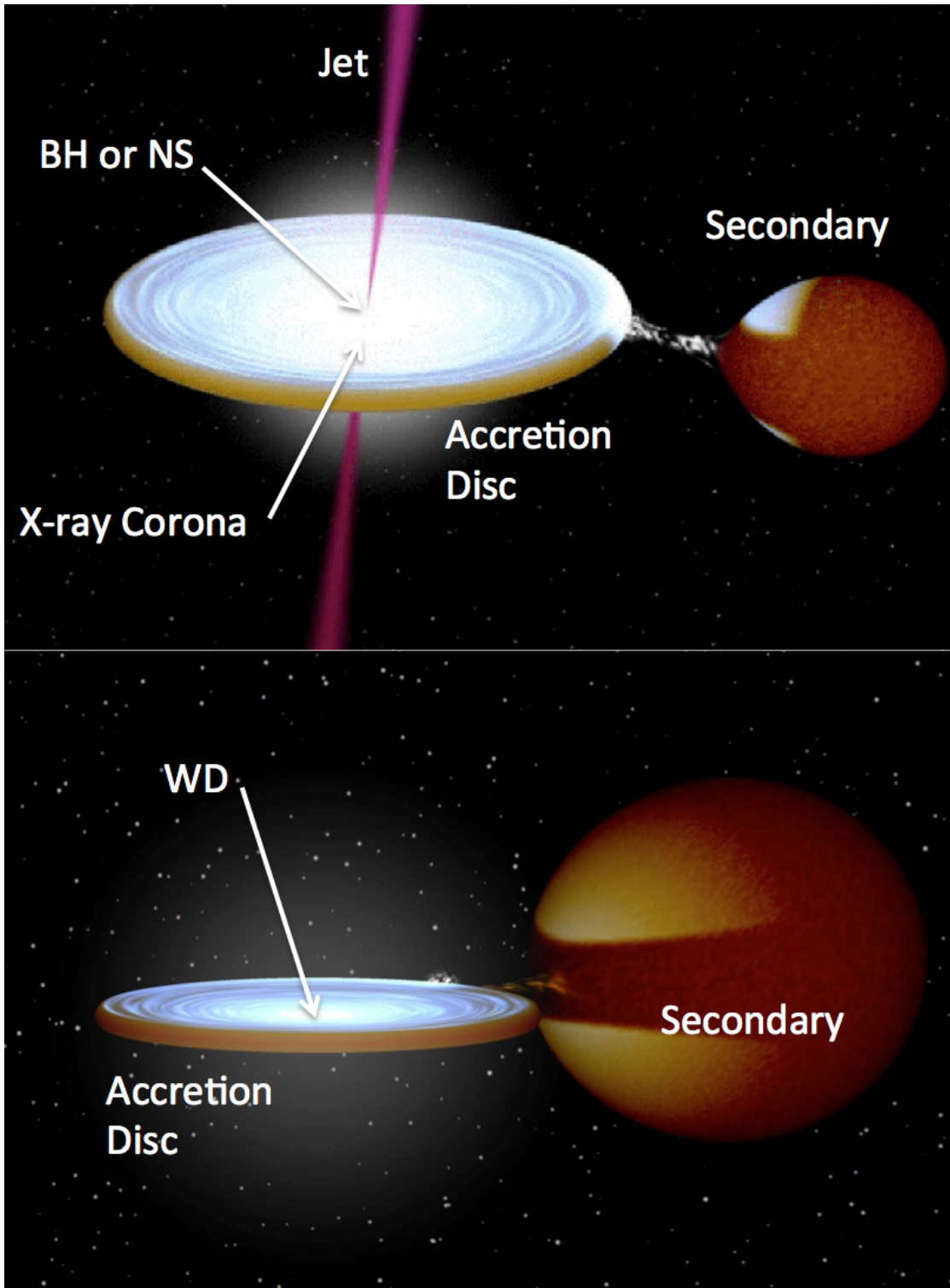


FIGURE 1.6: Credit: Rob Hynes. Artists impression of a low-mass X-ray binary (top) and cataclysmic variable (bottom). The key components are marked, and the clear similarity in overall structure is apparent.

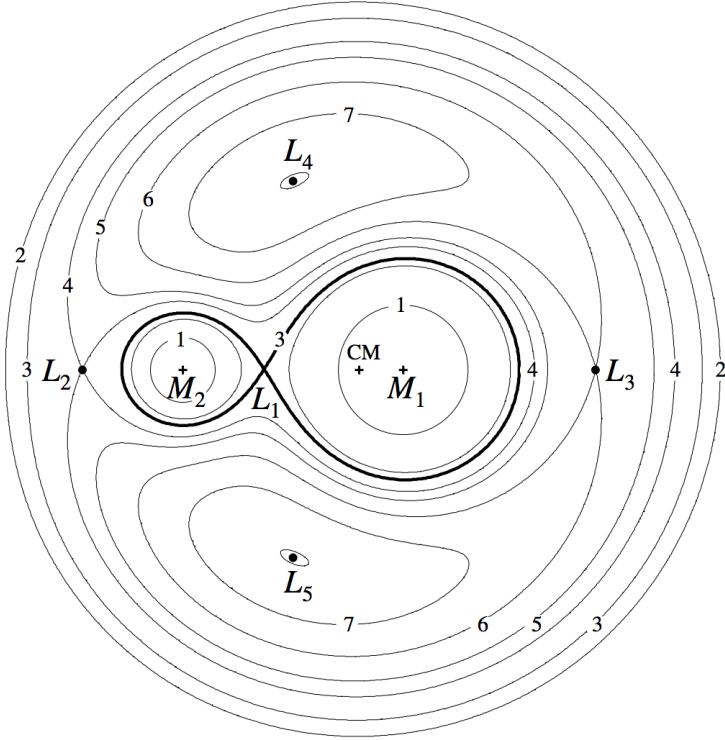


FIGURE 1.7: Credit: Frank et al. 2002. The Roche potential in a binary system for $q = M_2/M_1$ of 0.25. The Lagrangian points are marked, as are the locations of the individual and system centres of mass.

alternative is that the donor may expel material via a disc or radiatively driven stellar wind, allowing some of it to flow onto the compact object. Although accretion from a wind or circumstellar disc is common in high-mass X-ray binaries (HMXBs; e.g. [Bartlett 2013](#)), here I will focus on RLOF as it is more common in the systems that commonly exhibit high-state accretion discs and associated outflows. Two examples of these are shown in figure 1.6

1.2.1 Roche Lobe-Overflow

Let us consider a binary system, with masses M_1 and M_2 , at positions \vec{r}_1 and \vec{r}_2 . The Roche potential, Φ_R , in this system is then

$$\Phi_R = -\frac{GM_1}{|\vec{r} - \vec{r}_1|} - \frac{GM_2}{|\vec{r} - \vec{r}_2|} - 1/2(\vec{\omega} \times \vec{r})^2, \quad (1.21)$$

where $\vec{\omega}$ is the angular velocity of the binary and is a vector normal to the orbital plane. This potential is plotted in figure 1.7 for a mass ratio, $q = M_2/M_1$ of 0.25.

In the context of semi-detached binary systems, the most important region of the potential is the dumbbell shaped region enclosing the masses. Each of these enclosed regions is known as the ‘Roche lobe’ of the object and can be expressed approximately in terms of the mass ratio and separation of the system. An approximation for the size of the Roche lobe takes the form ([Eggleton 1983](#))

$$\frac{R_2}{a} = \frac{0.49q^{2/3}}{0.6q^{2/3} + \ln(1 + q^{1/3})}. \quad (1.22)$$

Here R_2 is the radius of a sphere with the same volume as the Roche lobe for the secondary star, which we can see depends only on q and the orbital separation, a . If this secondary expands enough to fill its Roche lobe, then matter will fall onto the other object. This process is known as Roche Lobe overflow (RLOF), and is vitally important in astrophysics. Although caused by stellar evolution, any accretion from RLOF will affect the mass ratio of the binary system and thus itself affects the evolution of binary systems. This helps determine the orbital period distribution of binaries (e.g. [Knigge et al. 2011](#)) as well as affecting the delay time distribution of Type Ia Supernovae, for which CVs are one of the progenitor candidates (e.g. [Wang & Han 2012](#)). It is also worth noting that the existence of gravitational waves has been required in models to explain the orbital period evolution of CVs since the 1960s ([Kraft et al. 1962](#)).

1.2.2 Cataclysmic Variables

Cataclysmic variables (CVs) are systems in which a WD accretes matter from a donor star via Roche-lobe overflow (see the ‘CV bible’, [Warner 2003](#)). CVs are not always dominated by their accretion luminosity; classical novae and super soft sources (SSS) emit mostly due to nuclear burning or detonation on the WD surface. Accretion dominated CVs – the focus here – can be classified according to the magnetic field strength (B) and photometric activity. Magnetic systems are classified as either ‘Polars’ ($B \gtrsim 10^7$ G) or ‘Intermediate Polars’ ($10^6 \lesssim B \lesssim 10^7$ G); in these systems the accretion flow inside the some critical radius (related to the Alfvén radius) is dominated by the WDs magnetic field (e.g. [Patterson 1994](#)). In polars this radius is large enough, due to the strong magnetic field, that no disc forms at all ([Liebert & Stockman 1985](#)). When $B \lesssim 10^6$ G then the accreting material can fall onto the WD via a disc, and the CV is classified

as non-magnetic. There are two main types of non-magnetic CVs; Dwarf Novae and Nova-like variables.

1.2.2.1 Dwarf Novae and the Disc-instability Model

Dwarf novae (DNe) are CVs that are characterised by repeated periods of quiescence and dramatic outburst. One of the most famous DNe is SS Cyg, whose light curve is shown in figure 1.8. The repeated outbursts can be clearly seen, and SS Cyg itself has been undergoing this behaviour for the full century for which it has been observed. A spectrum over the course of a typical outburst is shown in figure 1.9, and is characterised by the appearance of an optically thick accretion disc continuum – note the similarity to the stellar atmosphere disc spectrum computed in section 1.1.2.1, and to the intermediate inclination Nova-like variables discussed in the next section.

The leading candidate for explaining DN outbursts, and in fact the outbursts in low mass X-ray binaries or ‘soft X-ray transients’, is the disc-instability model (DIM; [Osaki 1974](#); [Lasota 2001](#)). In this model, a gradual increase in supply rate from the donor star (and hence surface density in the disc) causes the disc to heat up. Eventually, the disc hits a critical temperature, around 7000 K, and becomes ionized. Now the surface density in the disc can increase significantly, and the disc becomes geometrically thin and optically thick. Most importantly, it can efficiently undergo radiative cooling, and a significant increase in brightness is observed.

1.2.2.2 Nova-like Variables

Nova-like variables (NLs) are similar to DNe, except that the disc is always in a relatively high-accretion-rate state ($\dot{M} \sim 10^{-8} M_{\odot} \text{ yr}^{-1}$). NLs are therefore one of the best ‘laboratories’ for testing the steady-state accretion disc theory described in section 1.1.2.1. In the optical, NLs generally exhibit a series of H and He emission lines superposed on a blue continuum. In many cases, and particularly in the SW Sex subclass of NLs ([Honeycutt et al. 1986](#); [Dhillon & Rutten 1995](#)), these lines are single-peaked. This is contrary to theoretical expectations for lines formed in accretion discs, which are predicted to be double-peaked ([Smak 1981](#); [Horne & Marsh 1986](#)). *Low-state* CVs (dwarf novae in quiescence) do, in fact, exhibit such double-peaked lines ([Marsh & Horne 1990](#)).

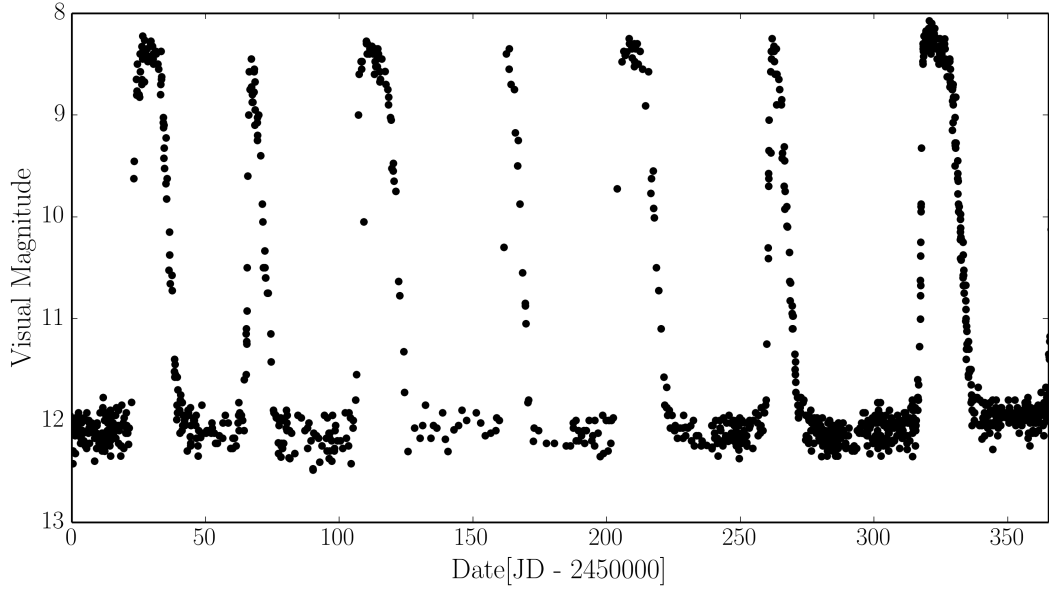


FIGURE 1.8: *Data: AAVSO.* A year in the life of SS Cyg, showing the characteristic repeated outbursts and periods of quiescence typical of a DN. SS Cyg has been undergoing this activity since it was first observed in 1896.

The UV spectra of NLs also show strong emission lines, and at low to intermediate inclinations dramatic blue shifted absorption lines can be seen in some objects. The emission line equivalent widths in both the optical and the UV show clear correlations with inclination (Hessman et al. 1984; Echevarria 1988; Noebauer et al. 2010). This can be seen clearly in figure 1.11, and links to the correlation between line strength and absolute magnitude found by Patterson (1984); that is, the decrease in equivalent width at low inclination is caused by an *increase* in continuum flux. This is discussed further in chapters 4 and 6, but also has relevance to AGN and quasar unification schemes mentioned later in this introduction. The optical and UV spectra are discussed in the context of winds in chapter 2.

1.2.3 Low Mass X-ray Binaries

Low Mass X-ray Binaries (LMXBs) are similar to CVs in structure (see figure 1.6), but the compact object is either a neutron star (NS) or black hole (BH). The accretion disc emits in the soft X-rays, and an additional hard X-ray power law is also seen in the spectrum. This hard component is normally attributed to Compton up-scattering of seed disc photons by some kind of ‘corona’ of hot electrons close to the BH (e.g. White et al. 1988; Mitsuda et al. 1989; Uttley et al. 2014). Although I do not study LMXBs

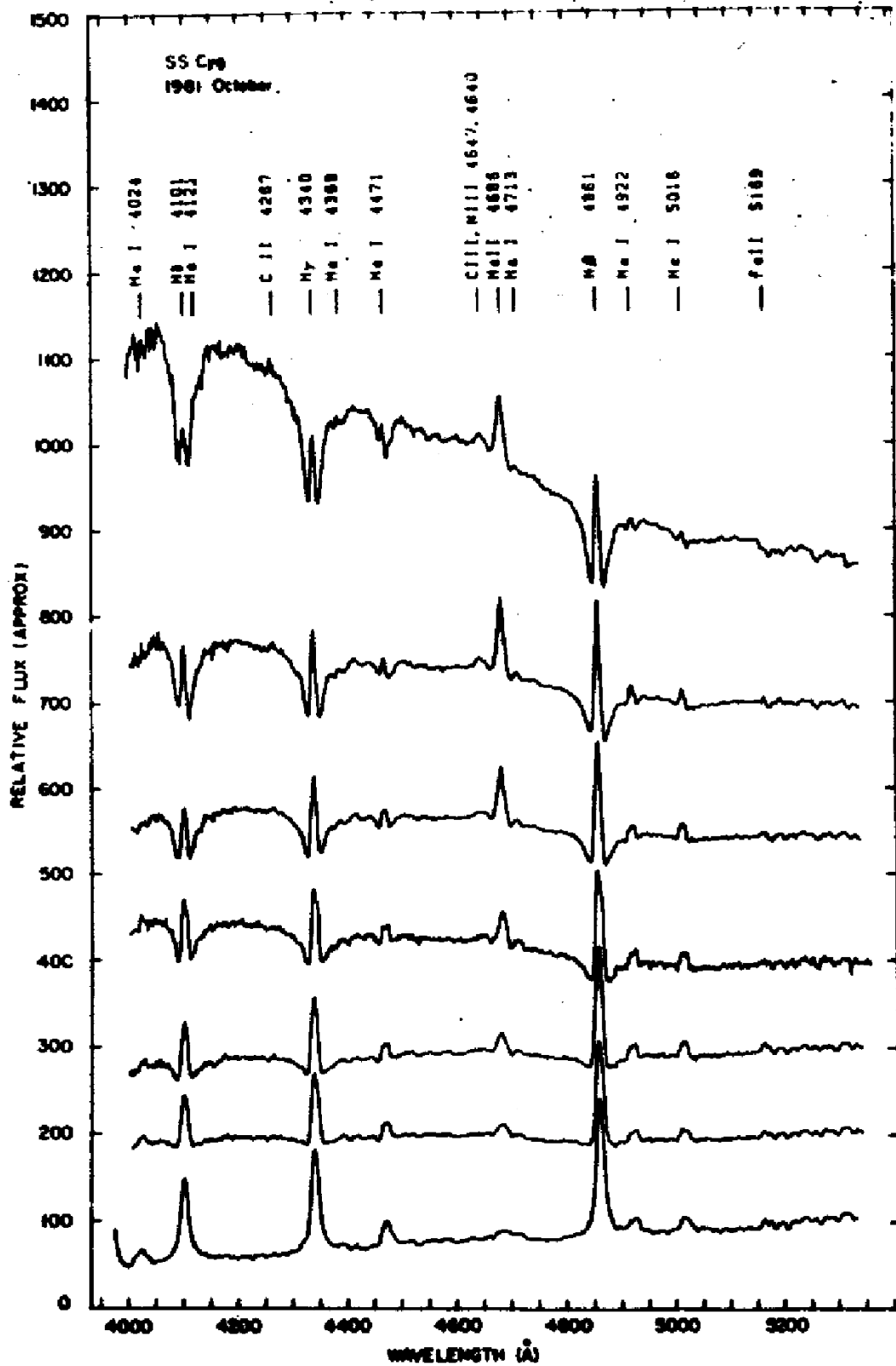


FIGURE 1.9: Credit: Hessman et al. 1984 / Dhillon et al. 1996. Spectra of SS Cyg during an outburst cycle, showing the evolution from minimum to maximum light. The rise is characterised by the appearance of an optically thick accretion disc spectrum. The flux scale is approximate.

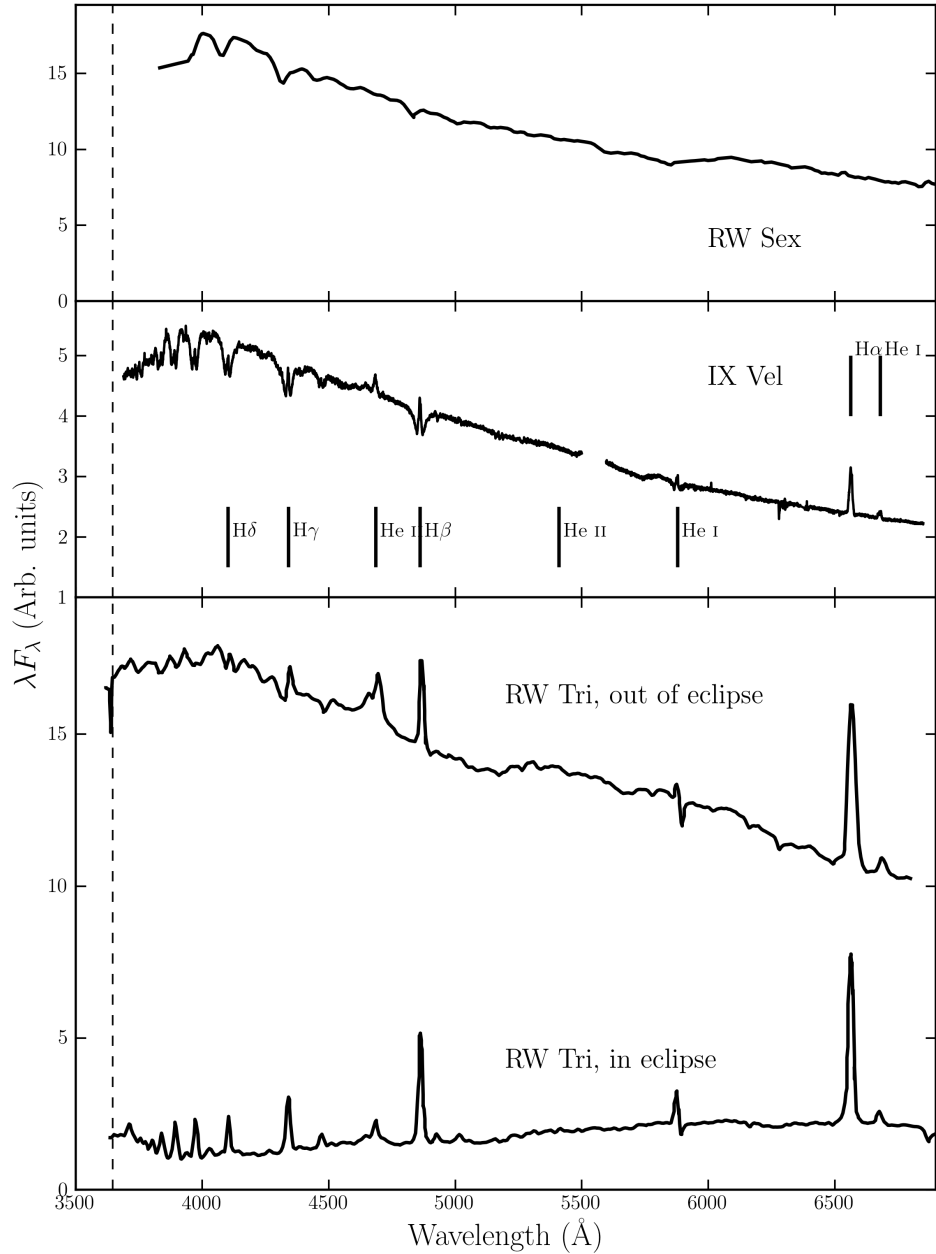


FIGURE 1.10: Optical spectra of three nova-like variables: RW Sex (top; Beuermann et al. 1992), IX Vel (top middle; A. F. Pala & B. T. Gaensicke, private communication) and RW Tri in and out of eclipse (bottom two panels; Groot et al. 2004). The data for RW Sex and RW Tri were digitized from the respective publications, and the IX Vel spectrum was obtained using the XSHOOTER spectrograph on the Very Large Telescope on 2014 October 10. These systems have approximate inclinations of 30° , 60° and 80° respectively. The trend of increasing Balmer line emission with inclination can be seen. In RW Tri strong single-peaked emission in the Balmer lines is seen even in eclipse, indicating that the lines may be formed in a spatially extensive disc wind, and there is even a suggestion of a (potentially wind-formed) recombination continuum in the eclipsed spectrum. I have attempted to show each spectrum over a similar dynamic range.

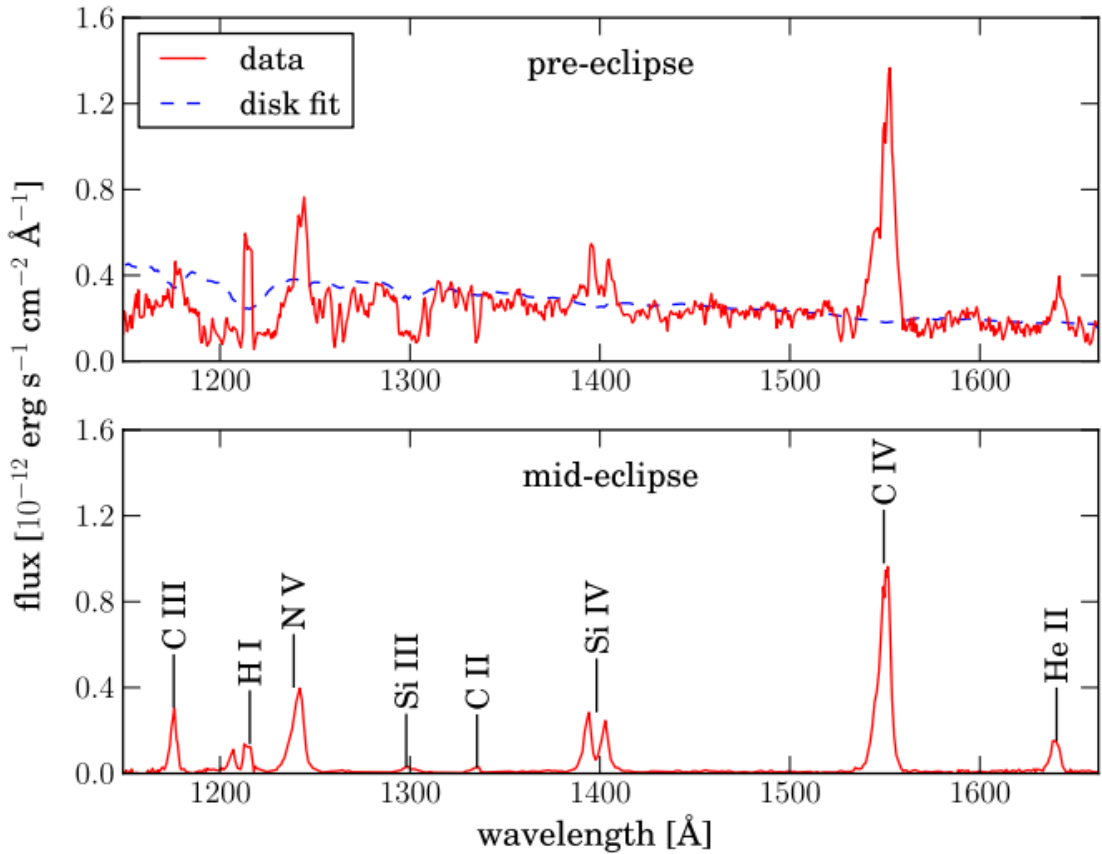


FIGURE 1.11: Credit: Noebauer et al. 2010. UV spectrum of RW Tri in and out of eclipse, showing strong lines in C IV λ 1550 and Ly α , among others.

directly in this thesis, it is instructive to discuss some of their observational appearance as it is relevant to the linksRE between accretion and outflow. The discovery that XRBs and CVs follow similar tracks on a hardness-intensity diagram ([Körding et al. 2008](#)) is particularly interesting in this regard, especially since [Ponti et al. \(2012\)](#) showed that broad Fe absorption lines are only seen in the soft-state high-inclination systems (see section 2.1.2). This implies that equatorial outflows are intrinsic to the accretion process. Although the driving mechanism is almost certainly different to CVs (e.g. [Díaz Trigo & Boirin 2015](#)), the similarity in general structure to models for CVs and quasars is striking.

1.3 Quasars and Active Galactic Nuclei

Spectra of AGN have now been studied for over 100 years, and we have known that they exhibit strong, broad emission lines since the first spectrum was taken by [Fath \(1909\)](#).

However, it wasn't until the work of [Seyfert \(1943\)](#) that the systematic classification of AGN really began, leading to the phrase 'Seyfert galaxy'. This label was applied to galaxies possessing a bright nucleus, spectroscopically characterised by a blue continuum and a series of strong emission lines. The first real physical insight into the extraordinary nature of AGN was provided by [Woltjer \(1959\)](#), who noted that (i) the nuclei must have sizes < 100 pc, based on the fact that they were unresolved and (ii) the mass of the nucleus must be very high, based on virial arguments. While both of these observations were based on simple arguments, the fact that these ultra-luminous celestial objects are both *compact* and *supermassive* is perhaps the defining insight into the nature of AGN.

Although the field of AGN study was established in the optical, radio astronomy also significantly furthered our understanding of AGN in the mid-20th century. A number of surveys, such as the Cambridge ([Edge et al. 1959](#)), Parkes ([Ekers 1969](#)) and Ohio ([Ehman et al. 1970](#)) surveys discovered a great many bright radio point sources distributed isotropically across the sky. These sources eventually became known as 'quasi-stellar radio sources' or *quasars*, and were soon identified to be coincident with bright optical sources or 'quasi-stellar objects' (QSOs) at high redshifts ([Schmidt 1963, 1965a,b](#)). Nowadays, the term quasar normally has very little to do with radio emission and is often used interchangeably with QSO. Indeed, throughout this thesis I shall refer to a quasar as simply a bright, massive AGN; one with sufficiently high luminosity that it dominates the emission from its host galaxy.

One of the main classifications schemes for AGN is a spectroscopic one, based on whether an object possesses broad emission lines in its spectrum, such as C IV broad H β and Ly α , in addition to the narrow lines that are always present. If these broad lines are seen, then the AGN is classed as type I, and if not, it is a type II; example spectra are shown in figure 1.12. These designations were originally applied to Seyfert galaxies ([Seyfert 1943](#)), but can also be used to classify the more luminous quasar class, despite the apparent difficulty in finding the expected number of type II sources ([Zakamska et al. 2003](#)). These classifications are complicated somewhat by narrow line Seyfert Is, which may be explained by super-Eddington accretion ([Done & Jin 2015](#)) or perhaps simply an orientation effect ([Baldi et al. 2016](#)), and the so-called 'true type II' AGN, in which the broad line region is absent ([Tran 2001; Shi et al. 2010](#)) rather than obscured (see next section). Despite the muddying of the waters, what was originally a clear dichotomy in

spectral type provided a profound motivation for attempting to *unify* AGN via geometric arguments.

1.3.1 AGN Unification and the dusty Torus

Although Seyfert had identified type 1 and 2 AGN, a physical explanation for this dichotomy was not forthcoming until a study by ([Antonucci & Miller 1985](#), AM85). They showed unambiguously that the nearby Seyfert 2 NGC 1068 is simply an obscured type 1 AGN, by finding that broad emission lines appeared in the spectrum of *polarised* flux. This provided the basis for the first successful attempt to unify AGN behaviour, as it elegantly explained the apparent disconnect between the two types of AGN as simply a viewing angle effect; at one angle, you could look directly into the broad line region (BLR) near the nucleus, but at Type 2 angles this region was hidden from view. The obscuring structure became known as the ‘torus’ ([Krolik & Begelman 1986](#)), due to its geometry, and it was soon realised that this structure may be made of dust, in which case it could also be responsible for the infra-red (IR) bump in AGN ([Neugebauer et al. 1979](#)).

([Urry & Padovani 1995](#), UP95) went further than the original unification model proposed by AM85 as they also tried to explain radio AGN phenomena. The picture they proposed is shown in figure 1.13. This model attempts to explain all of the types of AGN merely as a function of viewing angle and presence, or lack thereof, of a radio jet. Models such as this also describe the series of ‘bumps’ observed in AGN – the portions of the spectrum that dominate the luminosity, shown in figure 1.14. In most models, the ‘Big Blue Bump (BBB)’ is ascribed to thermal emission from an accretion disc, and the ‘Small Blue Bump’ to optically thin Balmer continuum and Fe II emission from the BLR. The latter can just be seen between $\sim 2000\text{\AA}$ and $\sim 4000\text{\AA}$ in the Seyfert 1 and quasar templates in figure 1.12. Our understanding of the BBB is still unsatisfactory (see section 1.4).

Since the seminal works by AM85 and UP95, the picture has become somewhat more complicated. Variable X-ray absorption has been detected in so-called ‘Changing look’ AGN ([Matt et al. 2003](#); [Puccetti et al. 2007](#)), even in NGC 1068 itself ([Marinucci et al. 2016](#)). Changes in type have also been seen in the optical lines; the broad H β component can dramatically disappear or reappear (e.g. [Tohline & Osterbrock 1976](#); [Cohen et al.](#)

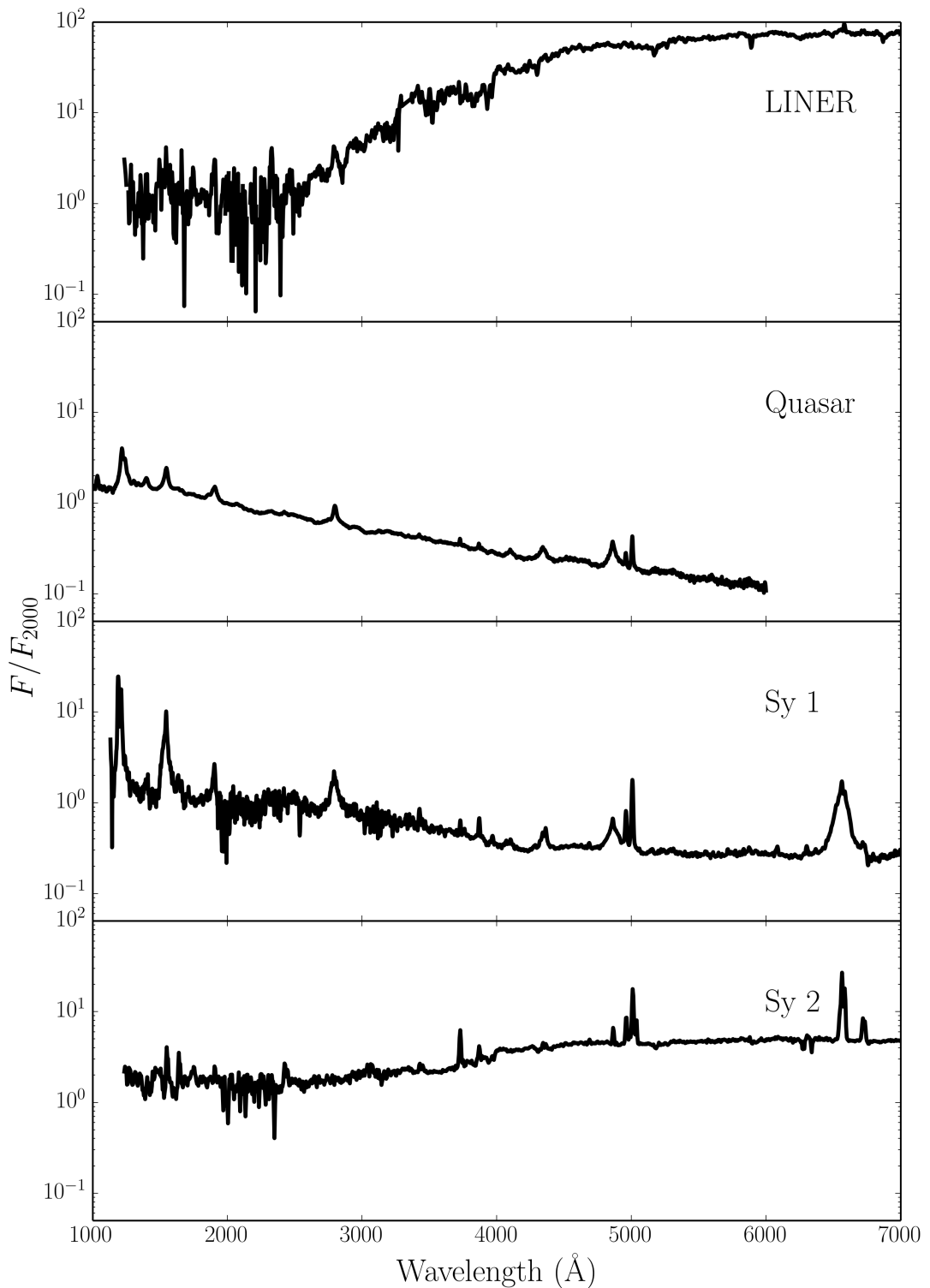


FIGURE 1.12: Template spectra, from the AGN atlas, for four common types of AGN.
Obtained from http://www.stsci.edu/hst/observatory/crds/cdbs_agn.html.

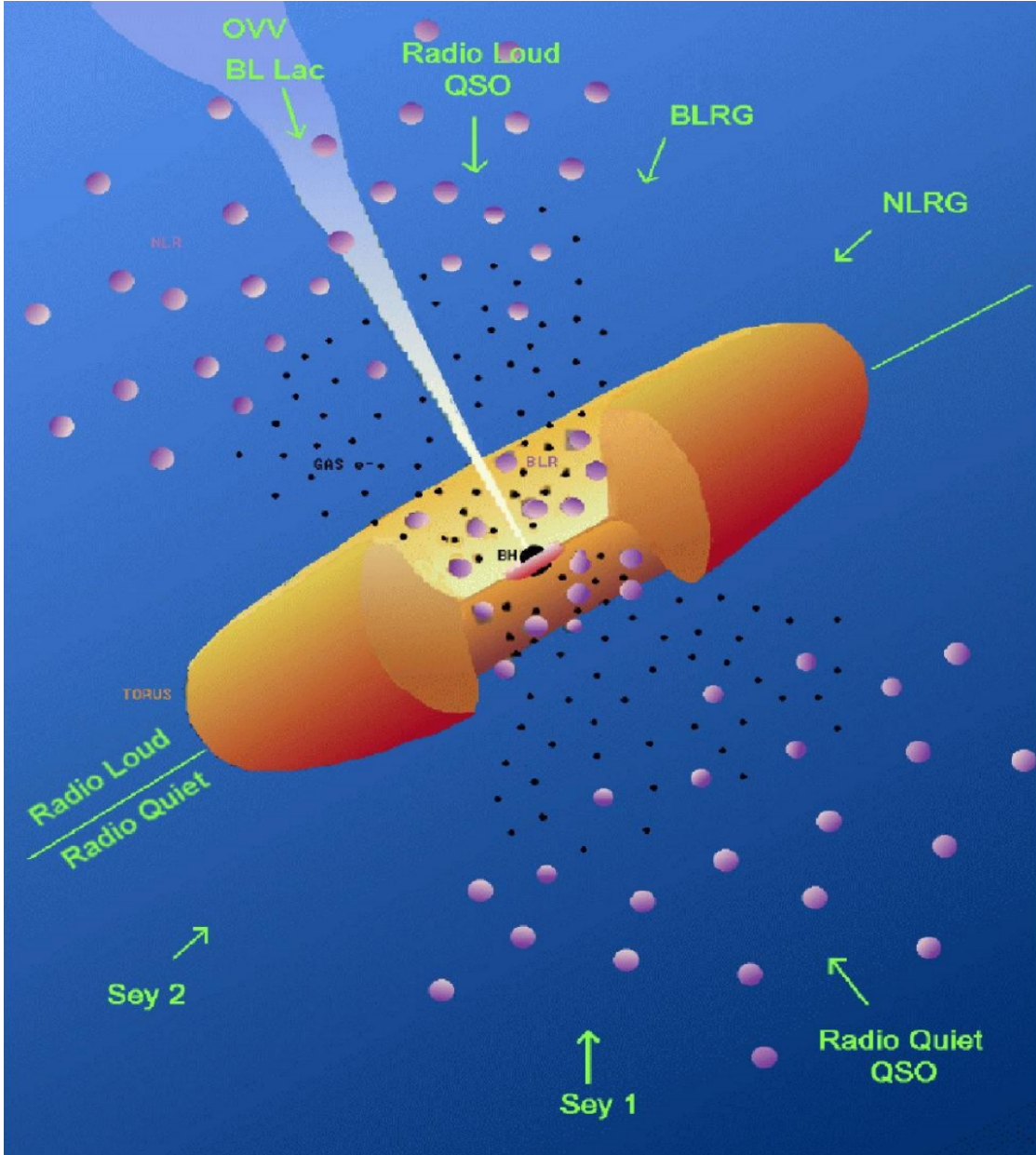


FIGURE 1.13: A unified scheme for AGN.

1986; Denney et al. 2014). The explanation for this could be variable absorption (Elitzur 2012) or linked to the accretion state of the disc. In the latter case, it has even been suggested that a disc wind could be directly responsible for this change in accretion state (Elitzur et al. 2014). Furthermore, dusty *polar* outflows have been found to be important IR emitters (Hnig et al. 2013), implying that, even when it comes to dust, the torus is not the whole picture. Despite these complications, the AGN torus unification picture still helps explain a lot of AGN behaviour, and represents a good framework to test with observations.

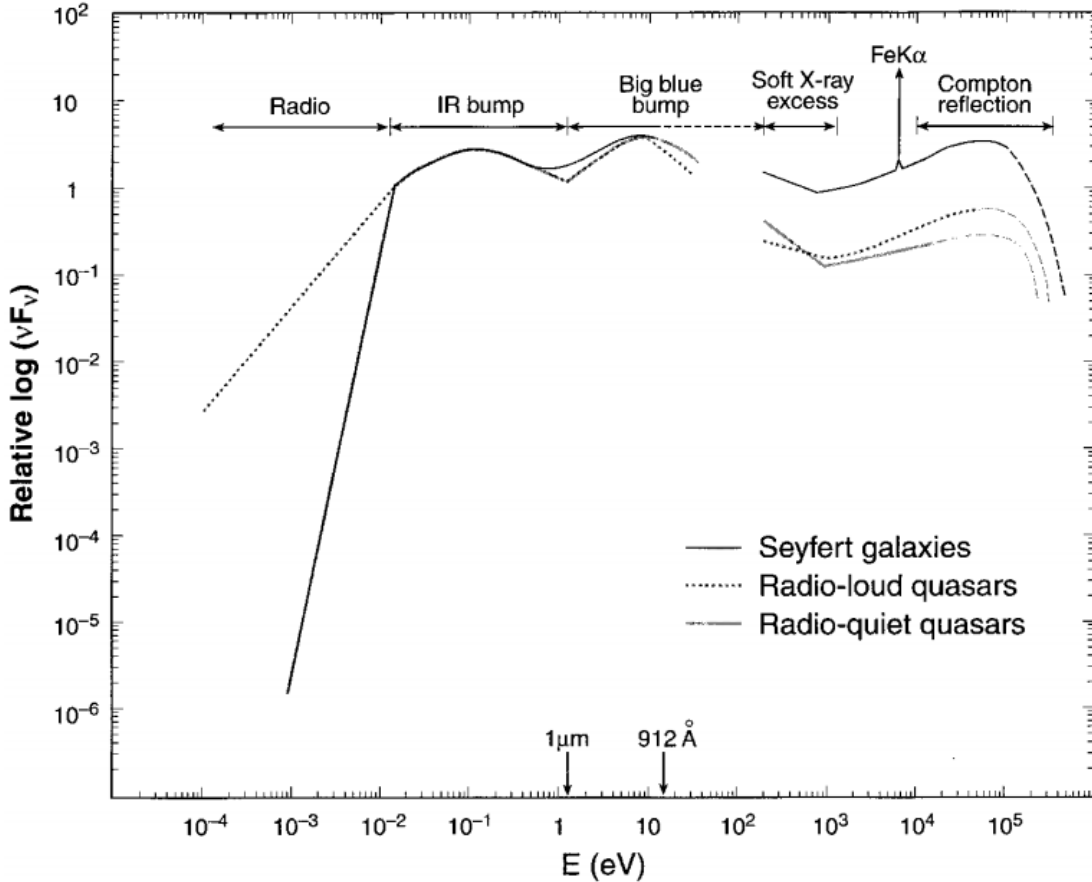


FIGURE 1.14: Credit: Koratkar & Blaes 1999 Approximate average broadband SEDs for a few types of AGN. The series of characteristic bumps can be clearly seen. The Soft-X-ray excess is also visible (see section 1.3.2.1).

1.3.2 X-ray Properties of AGN

Approximately 10% of the bolometric luminosity of AGN comes out in the X-ray band between ~ 0.1 and ~ 100 keV. Thus, AGN dominate the cosmic X-ray background (Madau et al. 1994). The hard X-ray emission follows a typical power law shape with spectral index -0.9 (e.g. Koratkar & Blaes 1999), widely considered, as in LMXBs, to come from a hot ‘corona’ of electrons, close to the BH, that upscatters disc seed photons (e.g. Haardt & Maraschi 1991). The compactness of this X-ray corona has been confirmed by microlensing (Chartas et al. 2009) and variability studies (Green et al. 1993; Crenshaw et al. 1996; Risaliti et al. 2007). Indeed, X-rays in AGN can be highly variable, both in terms of their intrinsic X-ray emission, but also due to changes in the absorption characteristics (Risaliti et al. 2002; Miller et al. 2008; Connolly et al. 2014). I discuss X-ray absorption in more detail, particular with respect to winds, in chapter 2.

The hard X-ray spectra AGN also tend to exhibit a number of reflection features. Typically, these consist of a strong Fe K α emission line and ‘Compton’ hump at high energies, which is produced by Compton down-scattering of high energy photons (Pounds et al. 1989; Nandra & Pounds 1994). It is still unclear exactly where these features originate, but a common interpretation is that they are caused by reflection off the inner parts of an accretion disc (Fabian et al. 1995; Iwasawa et al. 1996a; Reynolds 1999). If this is the case, and the broadening of the iron line is relativistic, then this would allow for measurements of the BH spin (Laor 1991; Iwasawa et al. 1996b; Dabrowski et al. 1997). This hypothesis is somewhat controversial. Multiple authors have found that many of the relativistic features supposedly imprinted by BH spin can in fact be explained by Comptonisation or absorption (e.g. Misra & Kembhavi 1998; Miller & Turner 2013), and radiative transfer modelling has shown that an outflow can naturally produce the characteristic broad red Fe K α wing (Sim et al. 2010a).

In Compton-thick AGN, the intrinsic continuum is heavily absorbed with columns of $N_H \sim 10^{24} \text{ cm}^{-2}$ – this absorption is normally attributed to the dusty torus, but Compton-thick winds could also contribute. Compton-thick AGN are required in large numbers so as to adequately explain the cosmic X-ray background (Setti & Woltjer 1989). In these sources, reflection features can actually dominate the X-ray spectrum (Alexander et al. 2011; Gandhi et al. 2013), but the Fe line is lowly ionized and on $\sim 0.1 \text{ pc}$ scales (Gandhi et al. 2015).

1.3.2.1 The Soft X-ray Excess

If one extrapolates the $\nu^{1/3}$ law from the BBB, and the power law in the hard X-rays, a curious excess of flux is often found in the soft X-rays in type 1 AGN (see figure 1.14, and Koratkar & Blaes 1999). This is known as the soft X-ray excess (SXXS), which is too hot to be explained by thermal disc emission, as a thin disc around an AGN should never approach the temperatures required. Many models have been proposed to explain this excess, including relativistically smeared photoabsorption (Gierliński & Done 2004, 2006), relativistically smeared line and free-free emission (Ross & Fabian 2005) and a variety of cool Comptonised component geometries such as an inner accretion flow (Magdziarz et al. 1998; Done et al. 2012) and thin layer on top of the disc (Janiuk et al. 2001). While the SXXS poses challenges to the simplest pictures of AGN, it may

also solve some of the issues, as some of the geometries proposed may help explain the accretion disc size problem (Done, private communication; see section 1.4) or inability to match observed spectra.

1.3.3 The Broad Line Region: Connection to winds and unification

In the UP95 unification model, the broad emission lines come from a series of virialised clouds close to the disc plane. As noted by (Murray et al. 1995, hereafter MCGV95), there are a number of problems with the BLR ‘cloud’ model, perhaps most notably that there is no obvious physical origin for a series of virialised clouds. Testing alternative models for the BLR is therefore important. Indeed, MCGV95 proposed a disc wind model in order to explain both BALs and BELs in quasars. A disc wind model was also discussed by Elvis (2000), who proposed a structure for quasars that attempted to explain much of the behaviour of luminous AGN merely as a function of viewing angle. Outflow models are discussed further in section 2. The philosophy of these models is that, before invoking additional degrees of freedom in a model, we should first test if known quasar phenomenology (winds) can explain other aspects of their observational appearance. I have illustrated this general principle with the ‘Occam’s quasar’ cartoon shown in figure 1.15. This is the picture that I will quantitatively test in the latter, quasar-focused sections of this thesis, and the general principle can even be applied to cataclysmic variables and other accreting objects.

1.4 The Current Understanding of the Disc Continuum

The SS73 model is still the most common way to fit accretion disc spectra and infer information about the underlying physics. However, a number of issues have been raised with the thin-disc model and its applicability to accreting systems.

1.4.1 The Spectral shape of CV discs

Attempts to fit the observed SEDs of high-state CVs with simple disc models have met with mixed success. In particular, the SEDs predicted by most stellar/disc atmosphere models are too blue in the UV (Wade 1988; Long et al. 1991, 1994; Knigge et al. 1998a)

OCCAM'S QUASAR: THE PRINCIPLE THAT IN EXPLAINING A QUASAR NO MORE ASSUMPTIONS SHOULD BE MADE THAN ARE NECESSARY.

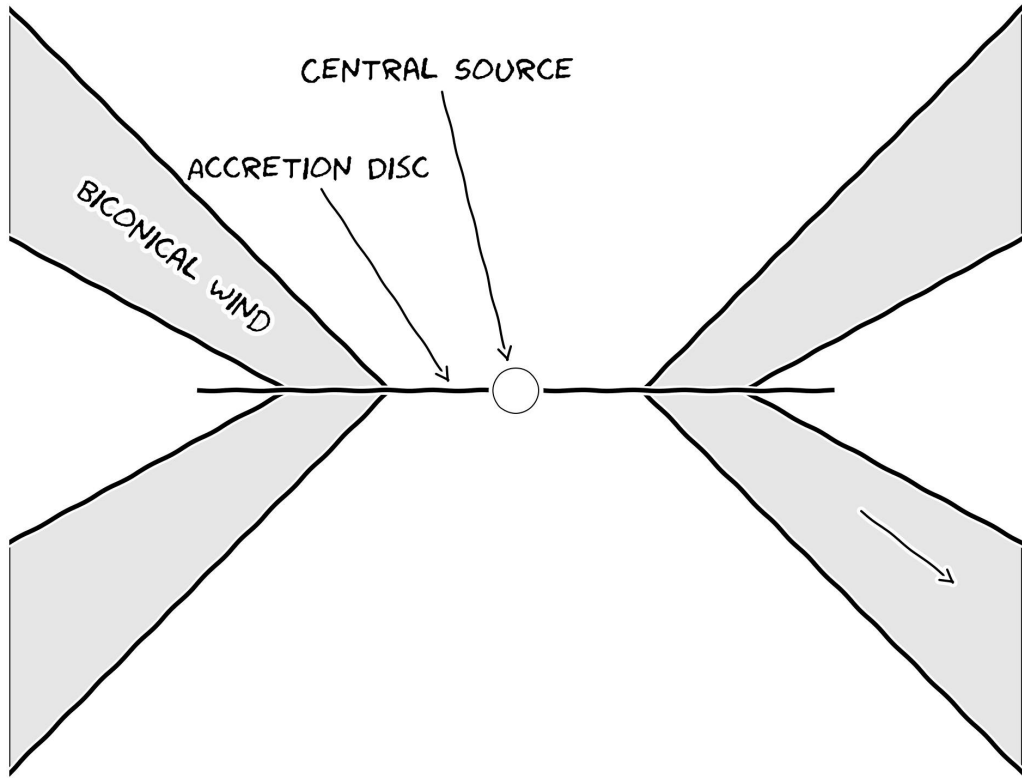


FIGURE 1.15: Occam's quasar. How far can this general picture take us when trying to explain the behaviour of quasars and other accreting compact objects?

and exhibit stronger-than-observed Balmer jumps in absorption ([Wade 1984](#); [Haug 1987](#); [La Dous 1989](#); [Knigge et al. 1998a](#)). One possible explanation for these problems is that these models fail to capture all of the relevant physics. Indeed, it has been argued that a self-consistent treatment can produce better agreement with observational data (e.g. [Shaviv et al. 1991](#); but see also [Idan et al. 2010](#)). However, an alternative explanation, suggested by [Knigge et al. \(1998b; see also Hassall et al. 1985\)](#), is that recombination continuum emission from the base of the disc wind might fill in the disc's Balmer absorption edge and flatten the UV spectrum.

Alternatively, it may just be that CV disks are never really in a steady state, and so we should only expect the $R^{-3/4}$ temperature profile to hold in a limited portion of the disc. From eclipse mapping, it has been shown that the inferred accretion rate increases with radius in NLs ([Rutten et al. 1992](#); [Horne 1993](#)). These results suggest that a non-radiative form of energy loss is present in the inner regions of the disc, of which

potential forms would be advection or mass loss. This is yet another piece of evidence that the understanding of accretion and outflow are intertwined, although hopefully not inextricably.

1.4.2 The Big Blue Bump in AGN

Does the SS73 model apply well to AGN spectra? There are contrasting views on the matter. On the one hand, [Antonucci \(2013\)](#) claims that “Most of the AGN community is mesmerized by unphysical models that have no predictive power”. Yet a recent spectral fitting study by [Capellupo et al. \(2015\)](#) concludes that “Altogether, these results indicate that thin ADs are indeed the main power houses of AGN”. So, what are the current problems when confronting thin disc models with observation?

1.4.2.1 The Accretion Disc Size Problem

One of the most interesting results of recent years relating to AGN and accretion discs is the discovery that the continuum emission region size is a factor ~ 3 larger than predicted by standard thin disc theory. This result has been found independently in both microlensing ([Morgan et al. 2010](#)) and reverberation ([Edelson et al. 2015](#)), and poses a challenge to the current best-bet model for the big blue bump in AGN. One proposed solution is that the discs in AGN are inhomogenous, consisting of individual clumps with independently varying temperatures ([Dexter & Agol 2011](#)), but this is very much still an active area of research. It is worth noting that the impact of winds on these results has not yet been properly quantified, something our team is currently trying to address ([Mangham et al. 2016](#))

1.4.2.2 Fitting AGN Spectra and the 1000Å Break

One of the *successes* of the thin disc model, when applied to AGN, is that we do observe a slope in the UV of $\alpha_{UV} = 0.32$, confirming the theoretical prediction of $\nu^{1/3}$. However, AGN spectra do not exhibit the *overall* spectral shape expected from theoretical predictions. It can be seen clearly in figure 1.12 that both the quasar and Seyfert spectra tend to peak in the UV, rather than the EUV. Furthermore, there is a characteristic break in AGN spectra at around 1000Å ([Lusso et al. 2015](#)), which does not scale with

BH mass or luminosity, as one might expect for a break associated with an accretion disc. There is also no evidence in AGN of the expected polarisation signatures from an optically thick disc atmosphere ([Stockman et al. 1979](#); [Antonucci 1988](#); [Antonucci et al. 1996](#)).

Despite these problems, recent work suggests that the thin disc model still has some potential. [Capellupo et al. \(2015\)](#) were able to fit a number of AGN spectra in the UV and optical with thin disc models, although successful fits were only found once they included effects such as Comptonisation and mass-loss, as well as correcting for extinction. BH spin also had a reasonable effect on the spectral fits, although it is somewhat difficult to constrain from spectral fitting alone. The 1000Å break has also been explained with a mass-losing disc ([Laor & Davis 2014](#)), and [Lusso et al. \(2015\)](#) suggested that incorrect IGM corrections may be exacerbating the effect. So, it would seem that, while many problems exist, it is not quite time to abandon the Shakura-Sunyaev ship just yet.

1.5 The Universality of Accretion

Accretion appears to be an important physical processes across ~ 10 orders of magnitude in mass. But is this process the same at all scales? Does any behaviour manifest in all accretion systems?

1.5.1 The RMS-flux relation

Broad-band variability is common in all types of accretion disc. It has been known for some time that there exists a linear relationship between the flux and absolute root-mean-square (rms) amplitude of this variability. This was discovered first in XRBs and AGN ([Uttley & McHardy 2001](#); [Uttley et al. 2005](#); [Heil et al. 2012](#)), but it has been shown more recently that the relationship extends to CVs and even YSOs ([Scaringi et al. 2012, 2015](#)). The relationship is not limited to one type of CV, as it is present in both NLs and DNe ([Van de Sande et al. 2015](#)).

The model that best reproduces this behaviour is the so-called ‘fluctuating accretion disc’ model ([Lyubarskii 1997](#); [Kotov et al. 2001](#); [Arévalo & Uttley 2006](#); [Hogg & Reynolds](#)

2015). It has been shown that additive processes cannot reproduce the behaviour, and a multiplicative mechanism is required (Uttley et al. 2005). Regardless of the mechanism, the rms-flux relation is one of the most clear-cut examples of a universal accretion phenomenon. It tells us that at least some of the behaviour in CV discs is present in AGN and XRBs, strengthening the argument that CVs should be used as ‘accretion laboratories’.

1.5.2 Accretion states and disc-jet coupling

Variable and transient sources are common in astrophysics, particularly when the sources are accreting. I have already mentioned the DIM and its applicability to LMXBs and CVs; it turns out that when you plot the colour and luminosity evolution over the course of an outburst cycle then they follow very similar tracks (see figure 1.16, Körding et al. 2008). The detection of radio jets is also intrinsically linked to the accretion state of the system (‘disc-jet coupling’), as jets only appear in the hard accretion state, to the right of the so-called jet line (Fender 2001; Fender et al. 2004). Körding et al. (2008) showed that this behaviour also occurs in CVs, as radio emission in the DN SS Cyg is also detected in the same region of colour-luminosity space. There is also a well-known correlation between radio and X-ray luminosities in low-hard states (Gallo et al. 2003).

This clear correlation with accretion state on HIDs has natural parallels with AGN.

The jet production mechanism in BHs in general is not well known. Theoretical work suggests that radio jets should be correlated with BH spin Penrose & Floyd (1971); Blandford & Znajek (1977), but whether such a correlation exists in LMXBs is controversial (Fender et al. 2010; Narayan & McClintock 2012). This has significant implications in AGN; the number of radio-loud AGN would imply a large fraction of them would then be rapidly spinning, with high radiative efficiencies. Further evidence that radio jets are not simply produced by RIAFs onto spinning BHs is found when one considers that NLs show evidence of extended synchrotron radio emission (Coppejans et al. 2015). This important result suggests that our understanding of jets is incomplete, and that the links between accretion state and jet production are fundamental, but unsolved. Disc winds may complicate, or simplify, matters, depending on your outlook (see chapter 2).

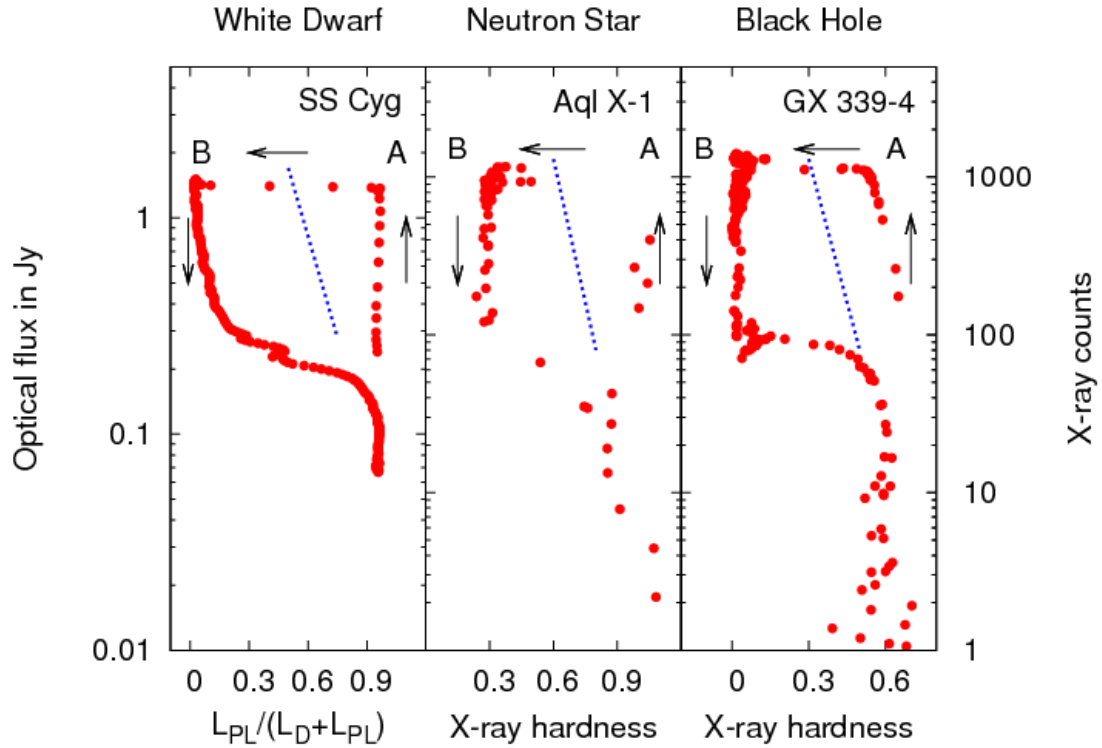


FIGURE 1.16: Credit: Kording et al. 2008. Caption.

1.5.3 A Global Picture

Clearly, accretion physics is relevant to a plethora of astrophysical phenomena, and at least some of the physics of accretion is applicable to *all* classes of accreting object. It would also appear that the outflowing material observed in accreting systems has a profound effect on the accretion process itself, and possibly significantly affecting the observational appearance of accretion discs (c.f. Elvis unification model). Hence, in the next chapter, I will detail the evidence for winds and discuss some of their theoretical considerations.

Chapter 2

Accretion Disc Winds

“A view of space, with an elephant
obstructing it”

Mike Vennart, Silent/Transparent

2.1 Observational Evidence

The observational evidence for mass-loaded outflows or winds is widespread across the entire astrophysical mass range and most of the electromagnetic spectrum. Before detailing the more compelling aspects of this evidence, it is pertinent to briefly discuss the ‘smoking gun’ used to unambiguously detect winds – the presence of blue shifted BALs or ‘P-Cygni’ profiles in an objects spectrum.

Figure ?? shows how a spherical outflow of significant opacity will cause these characteristic line profile shapes to form, as scattering out of the line of sight causes a dip in the blue wing of the line, while scattering into the line of sight from other portions of the outflow causes an increase in flux in the red wing of the line. The situation is much more complex in most astrophysical situations; for example, the geometry is rarely spherically symmetric, and the line is rarely a pure scattering case. Indeed, the potential for complicated radiative transfer effects and variety in line formation mechanisms is one of the reasons why 3D Monte Carlo radiative transfer simulations are necessary to effectively model disc winds (see section 3).

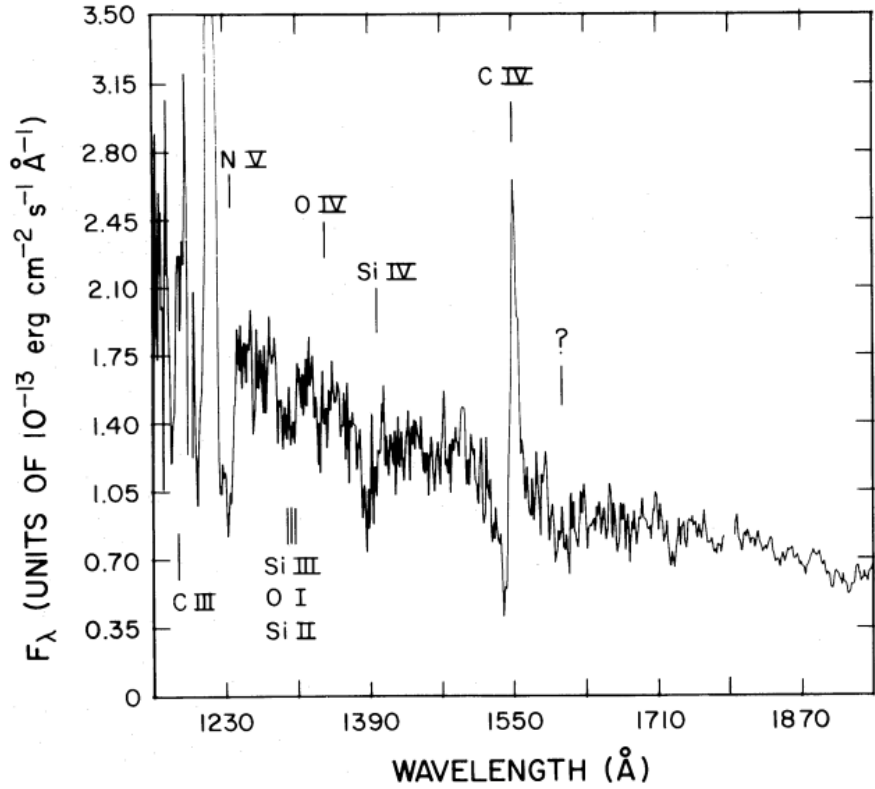


FIGURE 2.1: Credit: Cordova & Mason 1982. UV spectrum of the DN TW Vir during outburst. The P-Cygni profiles can be seen clearly, demonstrating that a strong, fast outflow is present in the system.

2.1.1 Cataclysmic Variables

It has been known for a long time that winds emanating from the accretion disc are important in shaping the ultraviolet (UV) spectra of high-state CVs (Heap et al. 1978; Greenstein & Oke 1982). The most spectacular evidence for such outflows are the P-Cygni-like profiles seen in UV resonance lines such as C IV λ 1550 (Cordova & Mason 1982, ; see figure 2.1)). Considerable effort has been spent over the years on understanding and modelling these UV features (e.g. Drew & Verbunt 1985; Mauche & Raymond 1987; Shlosman & Vitello 1993; ?; Knigge & Drew 1997; Knigge et al. 1997; Long & Knigge 2002; Noebauer et al. 2010; Puebla et al. 2011). The basic picture emerging from these efforts is of a slowly accelerating, moderately collimated bipolar outflow that carries away $\simeq 1\% - 10\%$ of the accreting material. State-of-the-art simulations of line formation in this type of disc wind can produce UV line profiles that are remarkably similar to observations, as shown in figure 2.2.

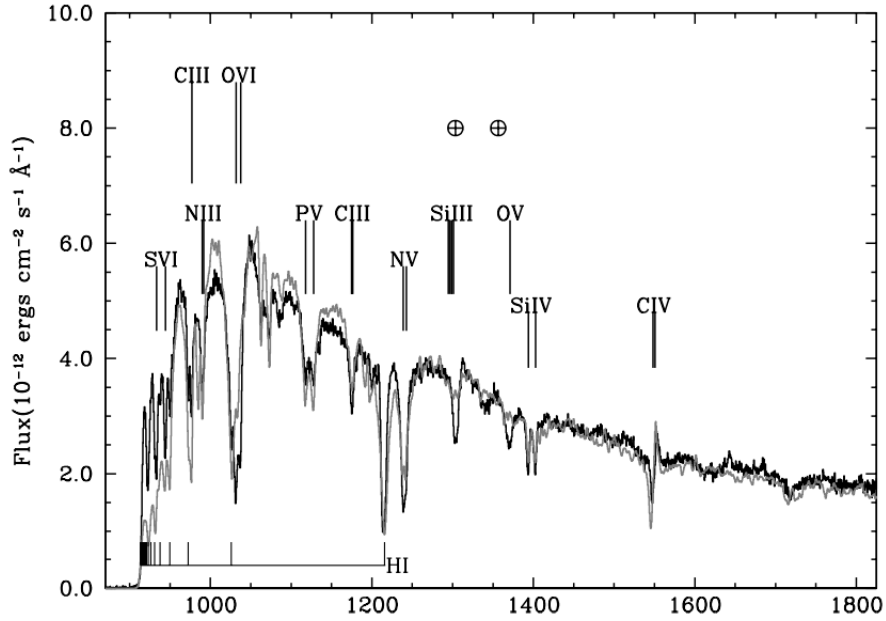


FIGURE 2.2: Credit: Long & Knigge 2002. UV spectrum of Z Cam, compared to a synthetic spectrum from MCRT simulations.

Much less is known about the effect of these outflows on the optical spectra of high-state CVs. Direct evidence of wind-formed lines comes from isolated observations of P-Cygni-like line profiles in H α and He I λ 5876, (Patterson et al. 1996; Ringwald & Naylor 1998; Kafka & Honeycutt 2004). However, the effect on the *emission* aspects of the optical spectrum is not well known. Murray & Chiang (1996, 1997) have shown that the presence of disc winds may offer a natural explanation for the single-peaked optical emission lines in high-state CVs, since they can strongly affect the radiative transfer of line photons (see figure ??). Stronger support for a significant wind contribution to the optical emission lines comes from observations of eclipsing systems. There, the single-peaked lines are often only weakly eclipsed, and a significant fraction of the line flux remains visible even near mid-eclipse (e.g. Baptista et al. 2000; Groot et al. 2004). This points to line formation in a spatially extended region, such as a disc wind (see section ??). It is also possible that a wind may affect the continuum emission of CVs, as described in section ??.

The effect of an accretion disc wind on the optical line and continuum emission of CVs is addressed directly, via radiative transfer modelling, in chapter 4.

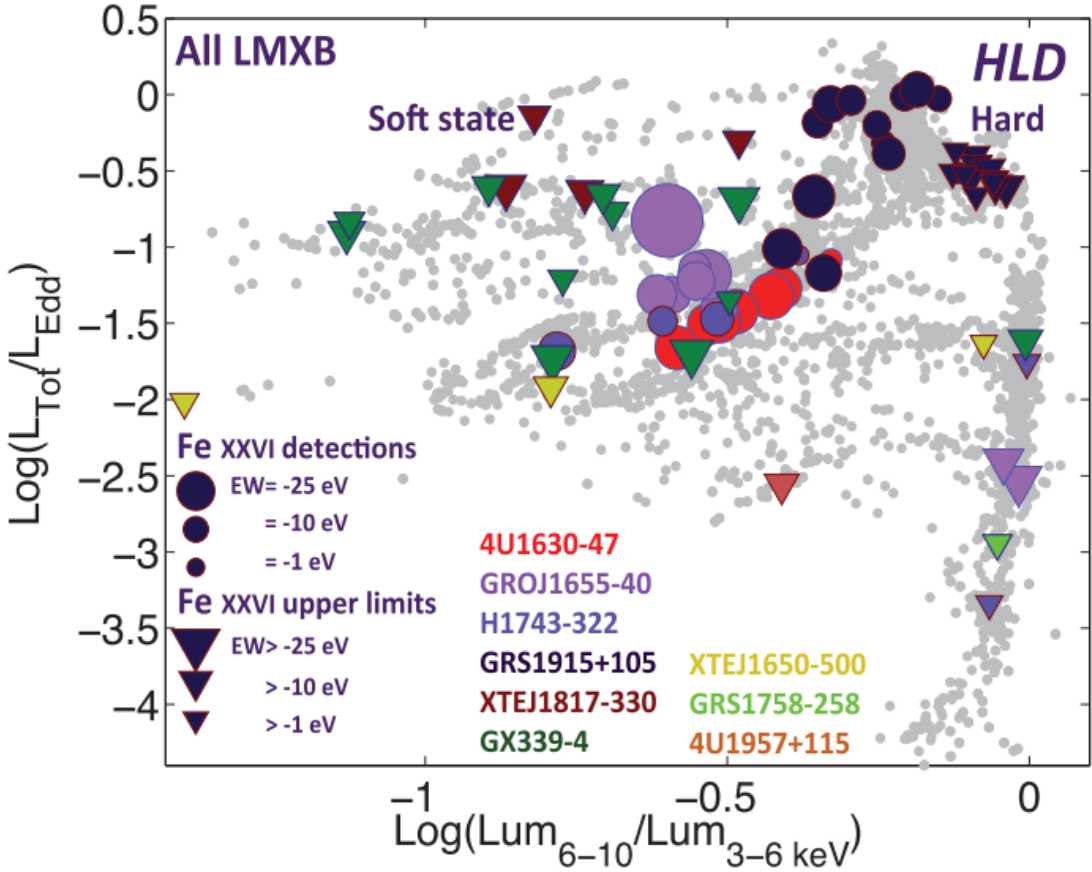


FIGURE 2.3: Credit: Ponti et al. 2012. HID demonstrating that winds appear in the soft states of LMXBs.

2.1.2 X-ray Binaries

Like CVs, evidence for fast outflows in LMXBs is not constrained to a single waveband. UV absorption in outflows was detected when Ioannou et al. (2003) observed C IV $\lambda 1550$ P-Cygni profiles with blueshifts of $\sim 1500 \text{ km s}^{-1}$. Shortly after, a series of papers found highly ionized Fe absorption with similar blueshifts and FWHM of around 1500 km s^{-1} (REFs). These absorption features tended to be detected in high-inclination, ‘dipping’ LMXBs, and this was confirmed in more sources by Ponti et al. (2012), who proposed an equatorial geometry based on this (see figure ??). The same study demonstrated (figure ??) that the winds only appeared in the soft, disc dominated accretion state, on the opposite side of the HID to the region where jets are common. This exciting result demonstrated how important winds are to our understanding of accretion, and required that we expand the discussion of accretion states to include ‘disc-jet-wind’ coupling.

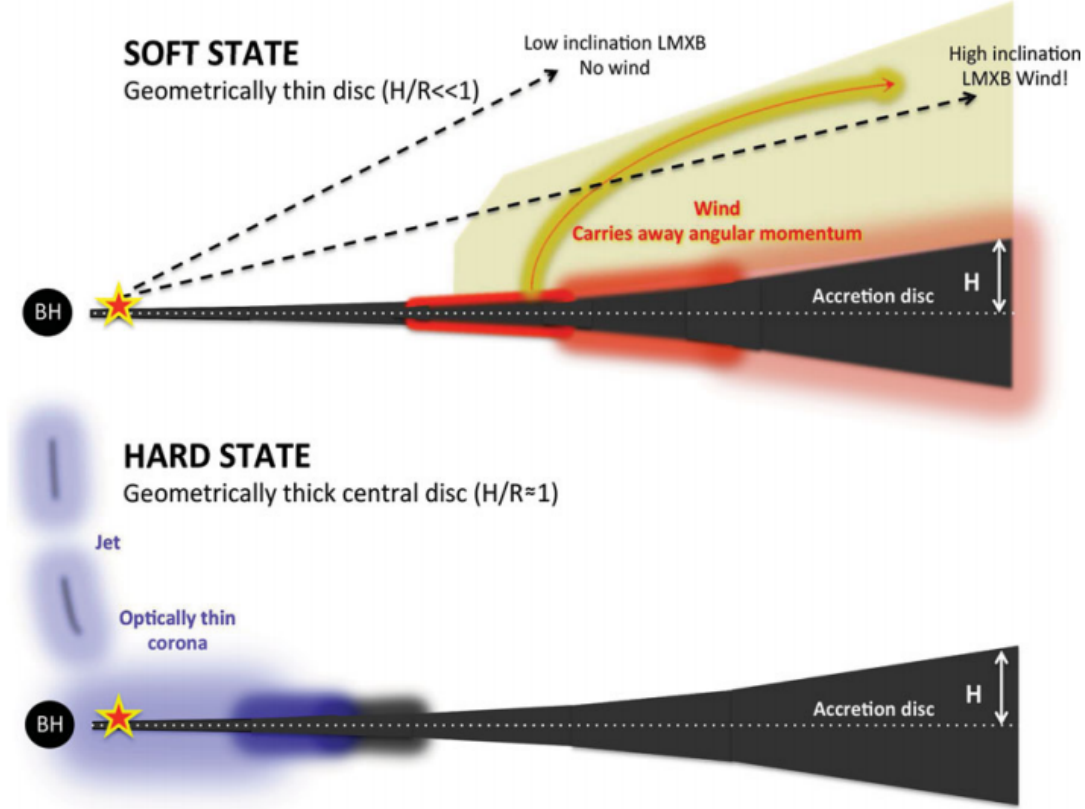


FIGURE 2.4: Credit: Ponti et al. 2012. A cartoon illustrating the expected geometry of soft-state LMXB winds.

2.1.3 AGN and Quasars

2.1.3.1 Broad Absorption Line Quasars

Perhaps the clearest evidence of outflows in AGN is the blueshifted ($\sim 0.1c$) broad absorption lines (BALs) in the ultraviolet seen in approximately 20% of quasars (Weymann et al. 1991; Knigge et al. 2008; Allen et al. 2011). The simplest explanation for the incidence of BAL quasars (BALQSOs) is in terms of an accretion disc wind. According to this paradigm, a biconical wind rises from the accretion disc and the BALQSO fraction is associated with the covering factor of the outflow. Polarisation studies suggest that the wind is roughly equatorial (Goodrich & Miller 1995; Cohen et al. 1995), although there is also evidence for polar BAL outflows in radio-loud (RL) sources (Zhou et al. 2006; Ghosh & Punsly 2007).

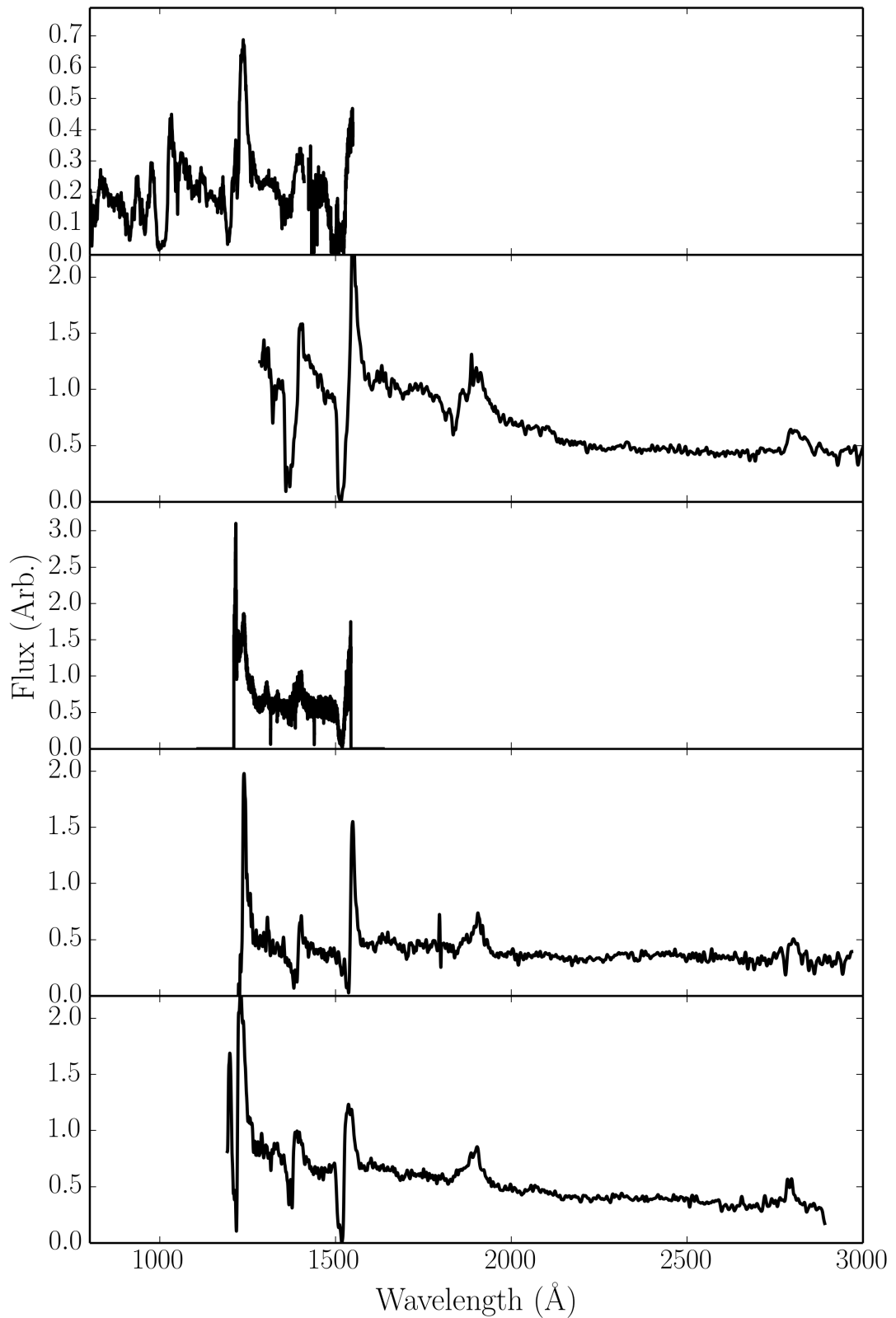


FIGURE 2.5: Five examples of BAL quasar spectra, from HST and SDSS.

2.1.3.2 Warm Absorbers

Warm absorbers (WAs) are regions of photoionized plasma responsible for some of the characteristic absorption features seen in the X-ray spectra of AGN (Reynolds & Fabian 1995). In particular, they produce photoelectric continuum absorption (e.g. Halpern 1984; Cappi et al. 1996; Kriss et al. 1996) and a series of narrow absorption lines in H-like and He-like ions of C, N, O, Si, Ne, and Fe (Kaastra et al. 2000), that appear in the soft X-rays. A wind origin is a common hypothesis for warm absorbers. Clear evidence for this comes from the measured blueshifts of the lines, typically on the order of $\sim 100 \text{ km s}^{-1}$ (REFs). X-ray absorption and warm absorbers are often variable (Fabian et al. 1994; Otani et al. 1996), which may be interpreted in terms of changing kinematics of an accretion disc wind (?). There is also evidence of contemporary UV and X-ray absorption in NGC 5548 (Kaastra et al. 2008), and as mentioned above BALQSOs are often absorbed in the X-rays. This suggests that the outflow phenomenon across a large range of ionization states and line energies is linked.

Warm absorbers can, in some cases, be modelled well with single component models (Kaastra et al. 2000), but often require multiple ionization state absorbers (e.g. Kriss et al. 1996; Orr et al. 1997; ?). If this is the case, then self-consistent ionization and radiative transfer models should really be used to model the spectrum (see e.g. chapter 3), as optically thin ionization parameter estimates will not capture the ionization and radiation physics. The collated observations point towards some kind of outflow with a stratified ionization structure, with $\log \xi \sim 0 - 2$, and densities on the order of 10^8 cm^{-3} . These physical conditions or scales are not well constrained, and the connection to other outflows is unknown. Timing observations will help to shed light on the properties of the mysterious, but ubiquitous, AGN warm absorbers (Silva et al. 2015).

2.1.3.3 Ultra-fast Outflows

As well as acting as warm absorbers, winds also imprint clear absorption features in highly ionized Fe K α lines in AGN such as PDS 456 (Reeves et al. 2003; Gofford et al. 2014; Matzeu et al. 2016), MCG-5-23-16 (Braito et al. 2007) and PG 1211+143 (Pounds & Reeves 2009; ?). These features are fairly common in Seyfert galaxies (Tombesi et al. 2010; Gofford et al. 2013). An example of such a feature is shown in figure 2.6 with a

simply spherical outflow model fit, from (?). The high velocities ($\sim 0.1c$) inferred from the line blueshifts have lead to these winds becoming known as ultra-fast outflows, or UFOs.

UFOs are characterised by ionization parameters of $\log \xi \sim 3 - 4$, and column densities of $N_H > 10^{22} \text{ cm}^{-2}$. Their high mass-loss rates and large energy budgets mean that they are natural candidates for AGN feedback (see section 2.5). Measurements of their kinetic luminosities suggest that UFOs do have sufficient energy to affect their host galaxy (Gofford et al. 2015), and a recent observation showed a molecular outflow in a UFO host galaxy, possibly driven by the UFO itself (Tombesi et al. 2015). As with WAs, many of the models used to constrain physical parameters are simplistic, and assume single ionization parameters, large covering factor and thin expanding shells of outflow. Under these assumptions, the kinetic luminosity can be estimated using

$$L_K = \Omega 4\pi r^2 n_e. \quad (2.1)$$

In reality, the absorber is probably much more complex, and full RT and photoionization simulations are required. In a series of papers, Sim et al. (2008, 2010a,b) carried out such calculations, and found reasonable verisimilitude with Fe line profiles could be achieved. However, as with many models for AGN, a holistic, broad wavelength range picture is still required.

2.1.4 Stellar Winds

Although stellar winds are clearly not accretion disc winds, they provide a useful, and better understood, testing ground for much of the physics of radiatively-driven outflows.

2.1.4.1 Clumping

2.2 Driving Mechanisms

Let us consider a parcel of ideal gas. By imposing nothing more than conservation of mass, energy and momentum on that parcel we can write down three equations of

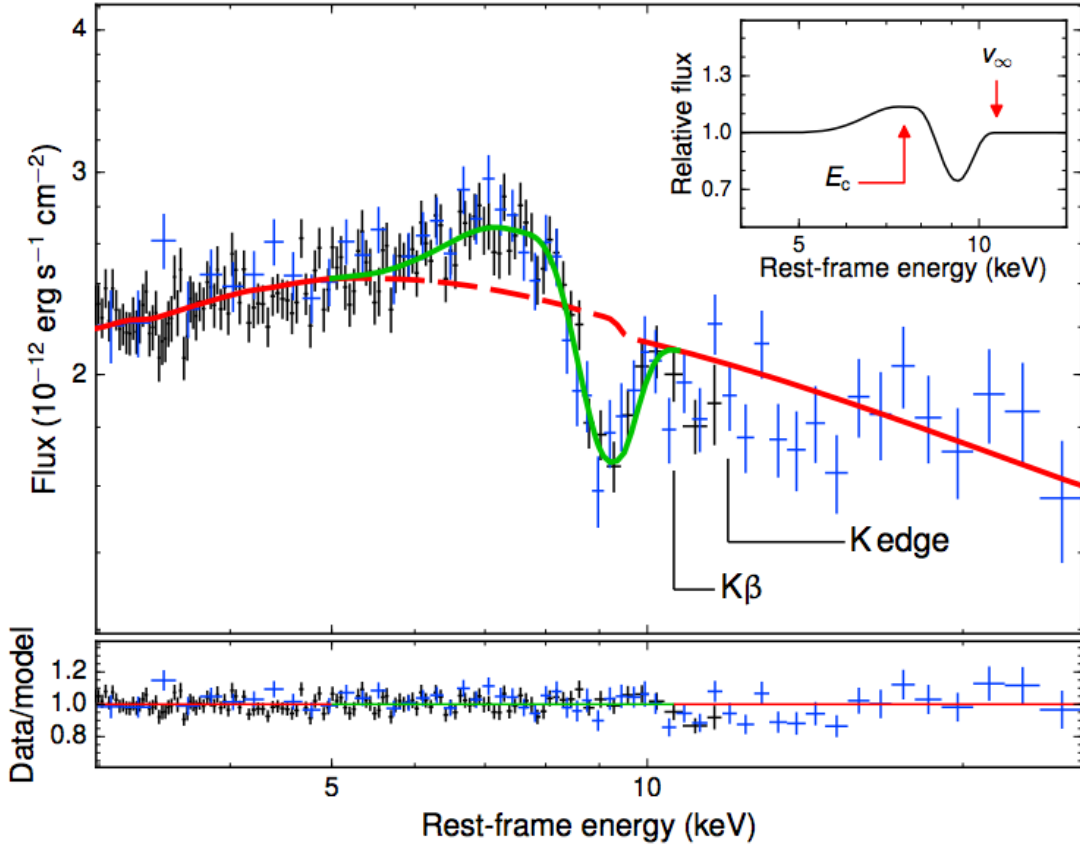


FIGURE 2.6: Credit: Nardini et al. 2015. X-ray spectrum of PDS 456 fitted with a P-Cygni profile from a spherical outflow model. *XMM-Newton* data is shown in black with two combined *NuStar* observations in blue.

hydrodynamics ¹

$$\frac{D\rho}{Dt} + \rho \nabla \cdot \vec{v} = 0 \quad (2.2)$$

$$\rho \frac{Dv}{Dt} = -\nabla P + \frac{1}{4\pi} (\nabla \times \vec{B}) \times \vec{B} + \rho \vec{F}_{rad} + \rho \vec{g} \quad (2.3)$$

$$\rho \frac{D}{Dt} \left(\frac{e}{\rho} \right) = P \nabla \cdot \vec{v} + \rho \mathcal{L} \quad (2.4)$$

Here D denotes a derivative within the comoving frame of the gas parcel, \vec{v} is the velocity, ρ is the gas density, \vec{B} is the local magnetic field, \vec{F}_{rad} is the radiation force

¹I stress that these equations are not used in hydrodynamic simulations in this thesis (see section ?, for example); they are discussed here because they provide a natural reference point for exploring potential driving mechanisms for winds in accreting systems.

per unit mass and \vec{g} denotes the gravitational acceleration vector. Equation 2.2 is the *continuity equation* and describes conservation of mass. Equation 2.3 is the *equation of motion* and describes conservation of momentum. Equation 2.4 is the *equation of energy conservation*. We can use equation 2.3 to neatly demonstrate how an outflow can be driven. I have deliberately written the equation so that all the force terms lie on the RHS. We can then see that for an outflow to be driven from an accreting object one simply needs one of the terms on the RHS to dominate over gravity, $\rho\vec{g}$. These terms thus signify three potential driving mechanisms.

- Magnetic Forces, $\frac{1}{4\pi}(\nabla \times \vec{B}) \times \vec{B}$.
- Radiative Forces, $\rho\vec{F}_{rad}$.
- Thermal Pressure, $-\nabla P$.

We can now examine under what physical conditions (and in which corresponding astrophysical objects) we might expect these forces to overcome gravity and cause a parcel of mass to escape to infinity. In other words: *what might drive a wind?*

2.2.1 Thermal Winds

In hydrostatic equilibrium (HSE), thermal pressure balances gravity and no other forces are present, meaning that the equation of motion can be written as

$$\rho \frac{Dv}{Dt} = -\nabla P + \rho\vec{g} = 0 \quad (2.5)$$

Clearly, if the thermal pressure is then significantly increased then this equilibrium condition no longer holds. This can occur in accretion discs at temperatures in excess of $\sim 10^7$ K – where other forces are negligible compared to thermal pressure – and where the escape velocities are relatively low (i.e. far out in the disc). Due to the temperature and gravity scalings, this means that XRBs are natural candidates for showing evidence of thermally driven winds. The outer disc can be heated to the Compton temperature by the central X-ray source, potentially driving relatively high mass-loss rate outflows (Begelman et al. 1983; Woods et al. 1996). This driving mechanism has been proposed as a natural explanation for the ever-present equatorial outflows in soft state XRBs (Ponti

et al. 2012). However, they are much less likely candidates in CVs and AGN **Discuss scaling arguments with equations?**.

2.2.2 Radiatively Driven Winds

2.2.3 Line-driven Winds

2.2.4 Magnetic Winds

Magnetic fields are one of the main proposed mechanisms for transporting angular momentum outwards in the disc via the MRI. This would imply that magnetic fields are important in shaping accretion discs and makes them attractive as a driving mechanism for disc winds.

There are two main ways in which magnetic forces can drive an accretion disc wind. Historically, the most popular idea has been the ‘bead on a wire’ mechanism proposed by (Blandford & Payne 1982). In this model, the *poloidal* magnetic field is dominant, and

2.3 Accretion Disc Wind Models

Describe a series of wind models. Elvis, Proga, CV winds, De kool and Begelman, some stratified and clumpy flows.

2.4 A Kinematic Prescription

Describe our wind model in detail. SV93, H13, M15, M16

2.5 The really, really big picture: AGN Feedback

The event horizon of a $10^9 M_\odot$ BH is approximately 10^{15} cm, a billionth of the size of a typical galactic bulge. This is roughly the difference in size between a small coin and

the Earth. Even the sphere of gravitational influence of the BH is roughly 1000 times smaller than the size of the galactic bulge. Despite this vast difference in scale, there are multiple pieces of evidence that the physics on the scale of the gravitational radius of the BH really does affect the evolution and dynamics of its host galaxy. When considering the energetics of accretion this becomes less surprising. The binding energy of a galactic bulge is

$$E_{bulge} = M_{bulge} \sigma_*^2 \quad (2.6)$$

I shall briefly discuss the evidence for this statement, and assess the potential role of winds together with alternative mechanisms.

2.5.1 Observational evidence for feedback

Go over the various pieces of observational evidence for feedback and the role of winds.

Perhaps the most famous pieces of evidence for some kind of long-distance relationship between a central BH and its host galaxy are the $M_{BH} - \sigma_*$ and $M_{BH} - M_{bulge}$ correlations, shown in figures ?? and 2.8 respectively.

2.5.2 Radiative or quasar mode feedback

2.5.3 Kinetic or radio mode feedback

2.5.4 Alternative Explanations

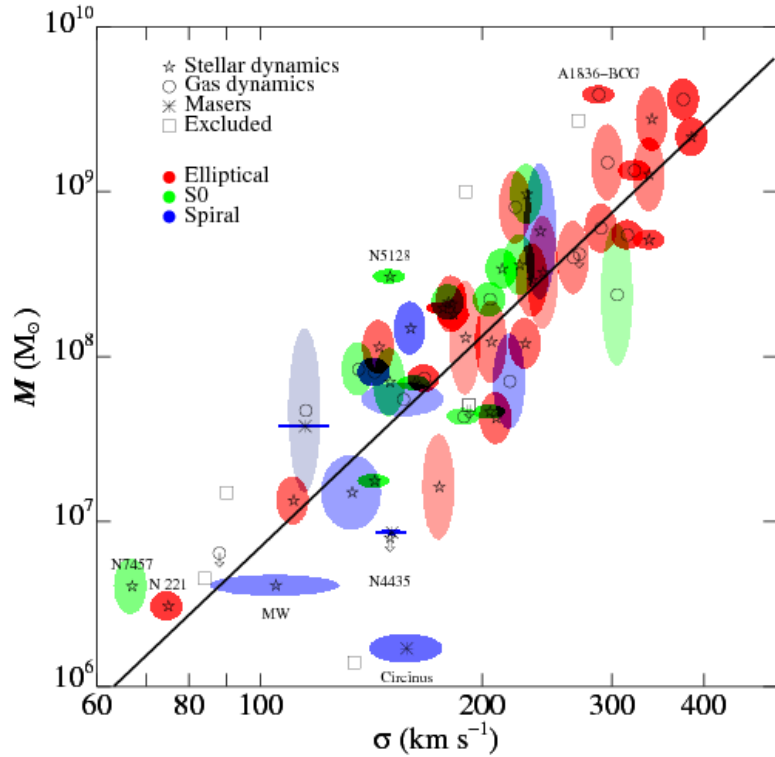


FIGURE 2.7: Credit: Gultekin et al. 2009. The $M_{BH} - \sigma_*$ correlation.

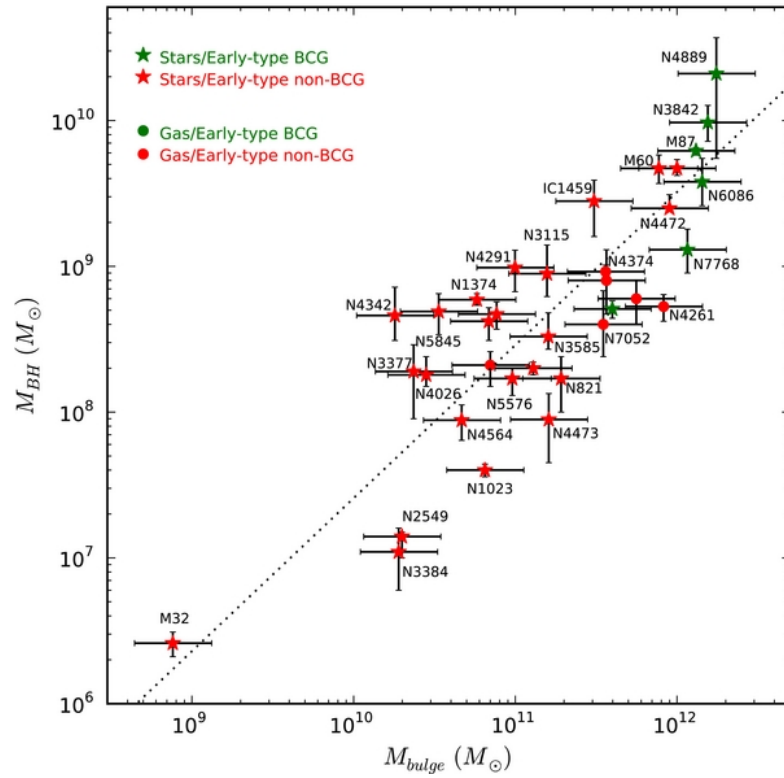


FIGURE 2.8: Credit: McConnell & Ma 2013. The $M_{BH} - M_{bulge}$ correlation.

Chapter 3

Quasar Emission Line Equivalent Widths as Probes of Orientation and Unification

3.1 Data Sample

To construct our sample, we start with the the Shen et al. (2010; hereafter S10) catalog of 105,783 quasars from the The Sloan Digital Sky Survey (SDSS) DR7. As we will use emission line diagnostics in this study, we must further divide this sample according

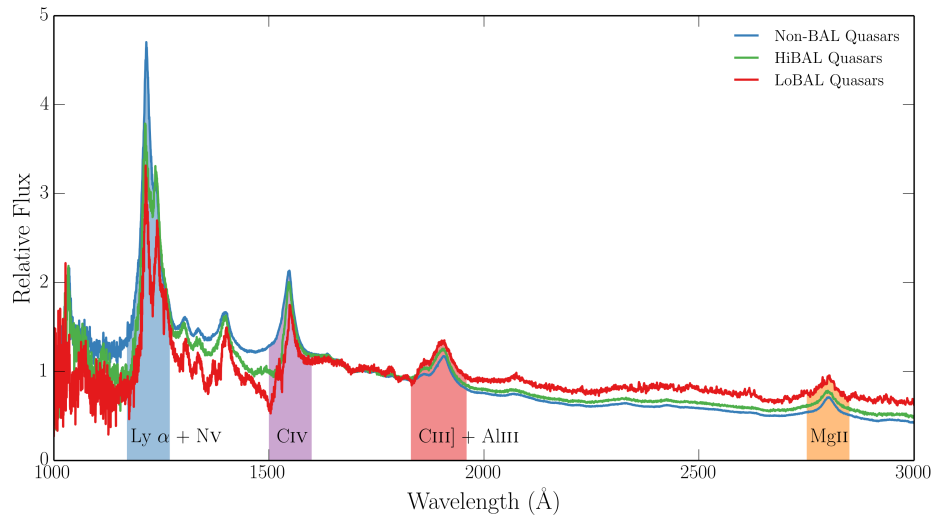


FIGURE 3.1: SDSS Composite spectra

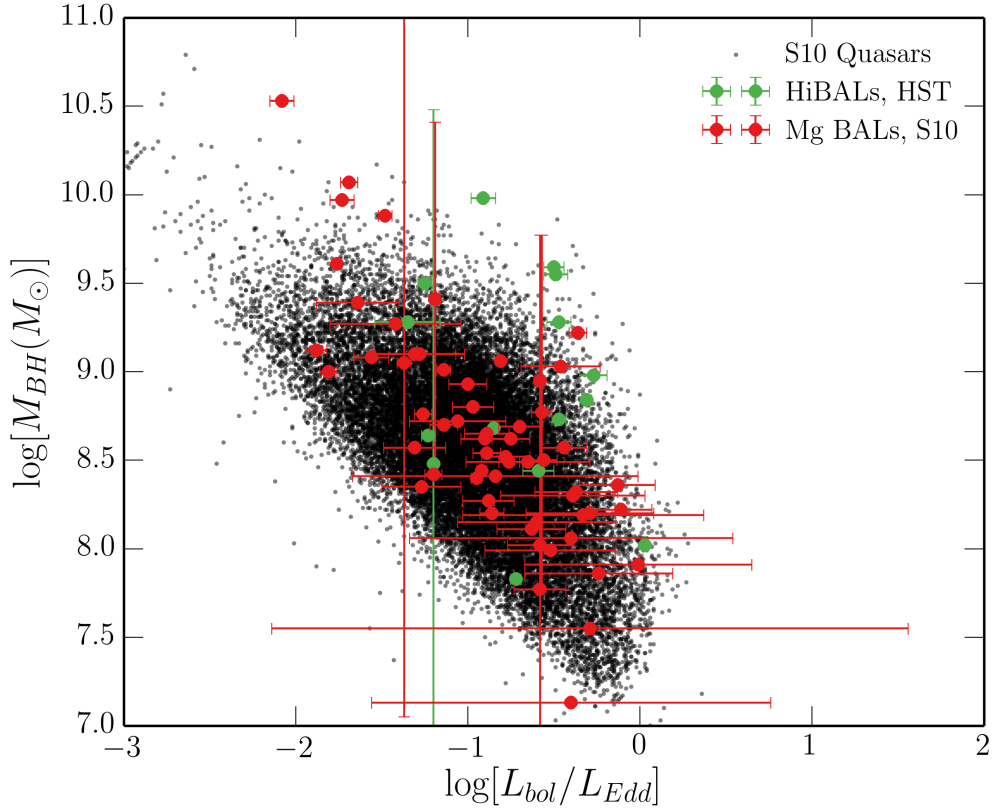


FIGURE 3.2: BH mass and Eddington fraction for the BAL samples plotted over the overall quasar sample from S10.

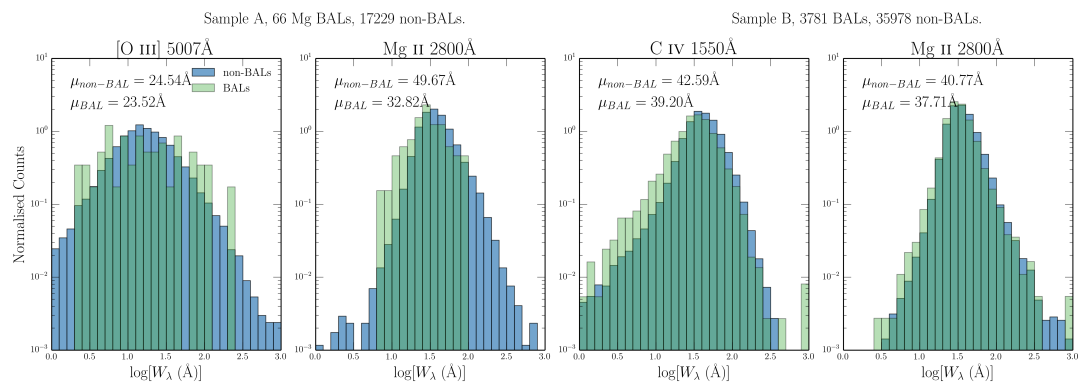


FIGURE 3.3: Histograms of equivalent widths for three emission lines from the two different samples.

to which emission lines are present in the SDSS wavelength range at a given redshift. Sample A contains all quasars within the redshift range $0.35 < z < 0.83$, such that the Mg II 2800A and OIII 5007A line EWs are both measured, and Mg II BAL identification is possible. Sample B contains all quasars within the redshift range $1.45 < z < 2.28$, such that the EWs and presence of BALs in Mg II 2800A and CIV 1550A are both measurable. The details of these samples are shown in table 1.

In attempting to draw broad conclusions about unification models as a whole, we would like to be able to construct a large homogenous dataset of *HiBAL* and non-BAL quasars with both OIII 5007A EWs. Unfortunately, the wavelength limits of SDSS do not allow this. One of the problems with using just LoBAL quasars as tests of unification is that there is evidence that they are drawn from a different population than normal quasars, perhaps suggesting an *evolutionary* origin. Examples include anomalously high LoBAL fractions in dust-reddened quasar samples ([Urrutia et al. 2009](#)) and infra-red selected samples ([Dai et al. 2012](#)); although see also [Lazarova et al. \(2012\)](#). To partially address this issue, we also build a small sample of HiBAL quasars in SDSS by cross-matching the S10 catalog with BALs identified in the HST COS archive. BALs were selected from the COS spectra using the balnicity index ([Weymann et al. 1991](#)), BI , defined as

$$BI = \int_{3000 \text{ km s}^{-1}}^{25000 \text{ km s}^{-1}} C \left(1 - \frac{f(v)}{0.9} \right) dv. \quad (3.1)$$

The constant $C = 0$ everywhere, unless the normalized flux has satisfied $f(v) < 0.9$ continuously for at least 2000 km s^1 , whereby C is set to 1. HST objects were designated as HiBALS by satisfying the condition that $BI > 0$ in one of CIV, NV, SiIV. The mass and Eddington fraction measurements from S10, with errorbars, are shown against the background distribution of all quasars.

Figure 2 shows histograms of a number of different emission line properties for samples A and B. As discussed by previous authors (e.g. [Weymann et al. 1991](#)), we find that BAL and non-BAL quasars really do seem to possess very similar emission line properties. The EW is related to the ‘face-on’ equivalent width, EW_0 by the equation

$$EW = EW_0 / \epsilon(\theta) \quad (3.2)$$

where θ is the viewing angle with respect to the symmetry axis and $\epsilon(\theta)$ is the ‘angular

emissivity function', which describes how the continuum luminosity from the disc varies as a function of viewing angle. For a foreshortened disc this is simply $\epsilon(\theta) = \cos \theta$.

Thus, if BAL quasars are viewed from a larger viewing angle on average then one would expect them to possess higher EWs, with a broader distribution. It is already apparent from figure 1 that the BAL distribution mean is not systematically higher than the non-BAL mean – in fact, it is lower. This is not expected from a model in which the continuum is foreshortened and BAL outflows are at all equatorial. This problem is examined further in section 3.3. First, we will examine the motivations for different forms of $\epsilon(\theta)$ in AGN and quasars.

3.2 The Angular Distribution of Emission from an Accretion Disc and Broad-Line Region

The most widely-used theoretical model for an accretion disc was proposed by Shakura & Sunyaev (1973; hereafter SS73). There are a number of well-documented problems when fitting AGN SEDs with SS73 accretion disc models (REFs), and there are also tensions with the ‘accretion disc size’ relation from time lags (Edelson et al. 2015) and microlensing (Morgan et al. 2010). Despite these problems, Capellupo et al. (2015) recently had some success fitting VLT XSHOOTER spectra of AGN when the effects of GR, mass-loss and comptonisation were included. In this section, we start by discussing the angular distribution of emission from an SS73 disc, before discussing opacity and GR effects. In order to explore these effects, we use AGNSPEC (Hubeny et al. 2000; Davis & Hubeny 2006; Davis et al. 2007). We stress that the discussion here is not limited to SS73 discs; the only real condition for the expected angular distributions derived here is that the disc is geometrically thin and optically thick.

3.2.1 Standard Thin Disc Models

A geometrically thin, optically thick disc will appear foreshortened and limb darkened (if temperature decreases with height from the central disc plane). Foreshortening is a simple $\cos \theta$ geometric effect, where θ is the inclination with respect to the vertical z

axis, which is perpendicular to the disc plane. Limb darkening, $\eta(\theta)$, is given by

$$\eta(\theta) = a(1 + b \cos \theta), \quad (3.3)$$

where a is a normalisation constant and b governs the strength of the limb darkening. $b = 3/2$, known as the Eddington approximation tends to give good agreement with solar observations (e.g. [Mihalas 1982](#)). The two effects can be combined to give an angular emissivity function, of

$$\epsilon(\theta) = a \cos \theta \left(1 + \frac{3}{2} \cos \theta\right). \quad (3.4)$$

3.2.2 Including GR, Comptonisation and Opacity Effects

In reality, limb darkening is not frequency independent and depends on the bound-free and bound-bound opacities in the disc. In addition, it has been shown that GR can ‘isotropize’ the radiation field in XRBs ([Zhang et al. 1997](#); [Muñoz-Darias et al. 2013](#)), in some cases overcoming foreshortening effects. To assess the impact of GR and disc opacities on $\epsilon(\theta)$ we use AGNSPEC models, which uses stellar atmosphere calculations to calculate the SED in a series of annuli, before using the KERRTRANS code to calculate the emergent SED by ray-tracing along Kerr geodesics. In Fig. 3.4, we show $\epsilon(\theta)$ as a function of θ for AGNSPEC models for minimally and maximally spinning BHs, compared to foreshortened and limb-darkened predictions for SS73 models. Clearly, there is very little effect; the accretion disc is still strongly anisotropic in the relevant wavebands.

3.2.3 Alternative Continuum Models: Irradiation and Truncated Discs

Alternative Models exist...

3.3 Predicted EW distributions compared to observations: A Monte Carlo approach

We assume $\epsilon(\theta) = \cos \theta$, as this is the conservative estimate.

Our Monte Carlo simulation undergoes the following steps:

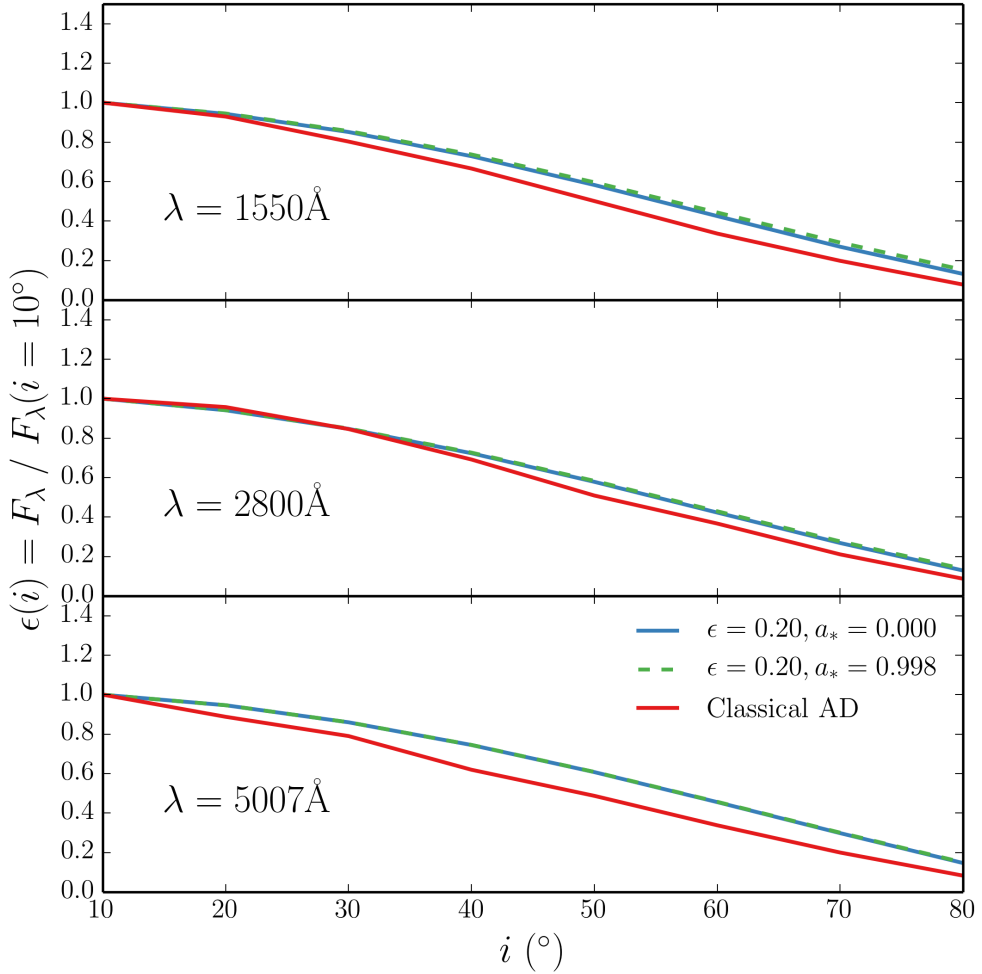


FIGURE 3.4: Monochromatic continuum luminosities from AGNSPEC and classical thin disc models.

1. A set of isotropic angles is chosen such that $P(\theta) \propto d\Omega(\theta)$. If $\theta_{min} < \theta < \theta_{max}$ then the fake object is flagged as a mock BAL. If $\theta < \theta_{min}$ then the fake object is designated a non-BAL, and otherwise the object is ignored. To be included in the sample, the object also has to survive a selection test based on a arbitrary flux selection limit, to simulate the distribution of angles in a flux-limited sample.
2. We then construct our best estimate of the intrinsic (i.e. ‘face-on’) EW distribution for non-BAL quasars. This is done via a χ^2 minimisation, by finding the gaussian with μ and σ which best reproduces the observed distribution when convolved with the non-BAL angles generated in the previous step. a χ^2 minimisation.

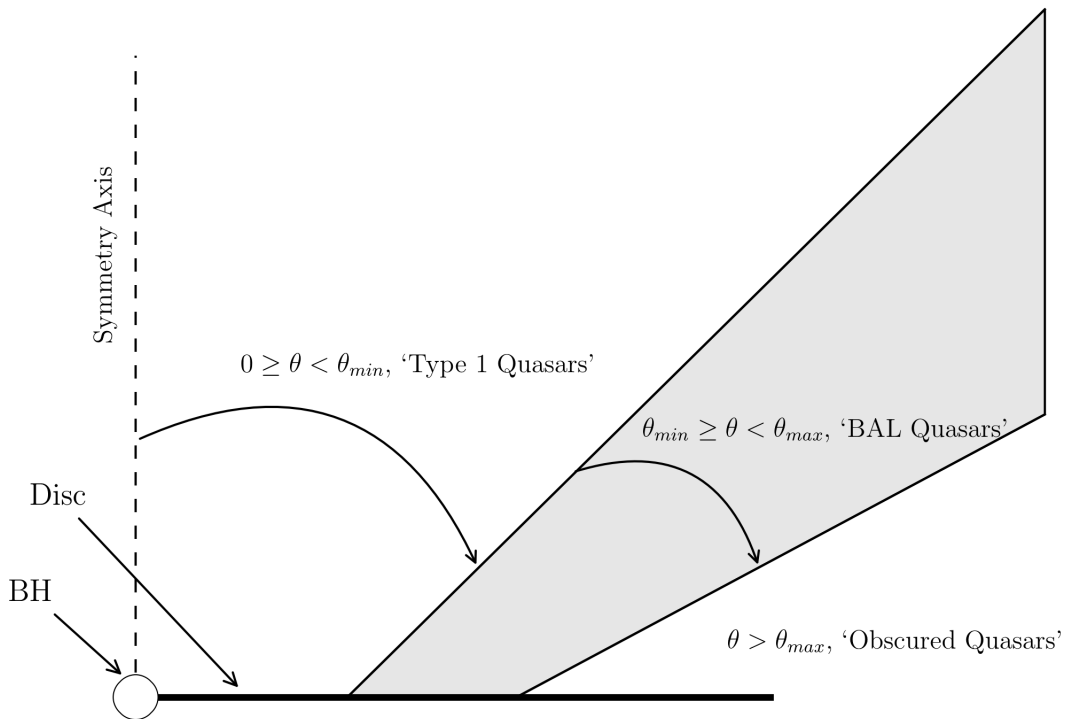
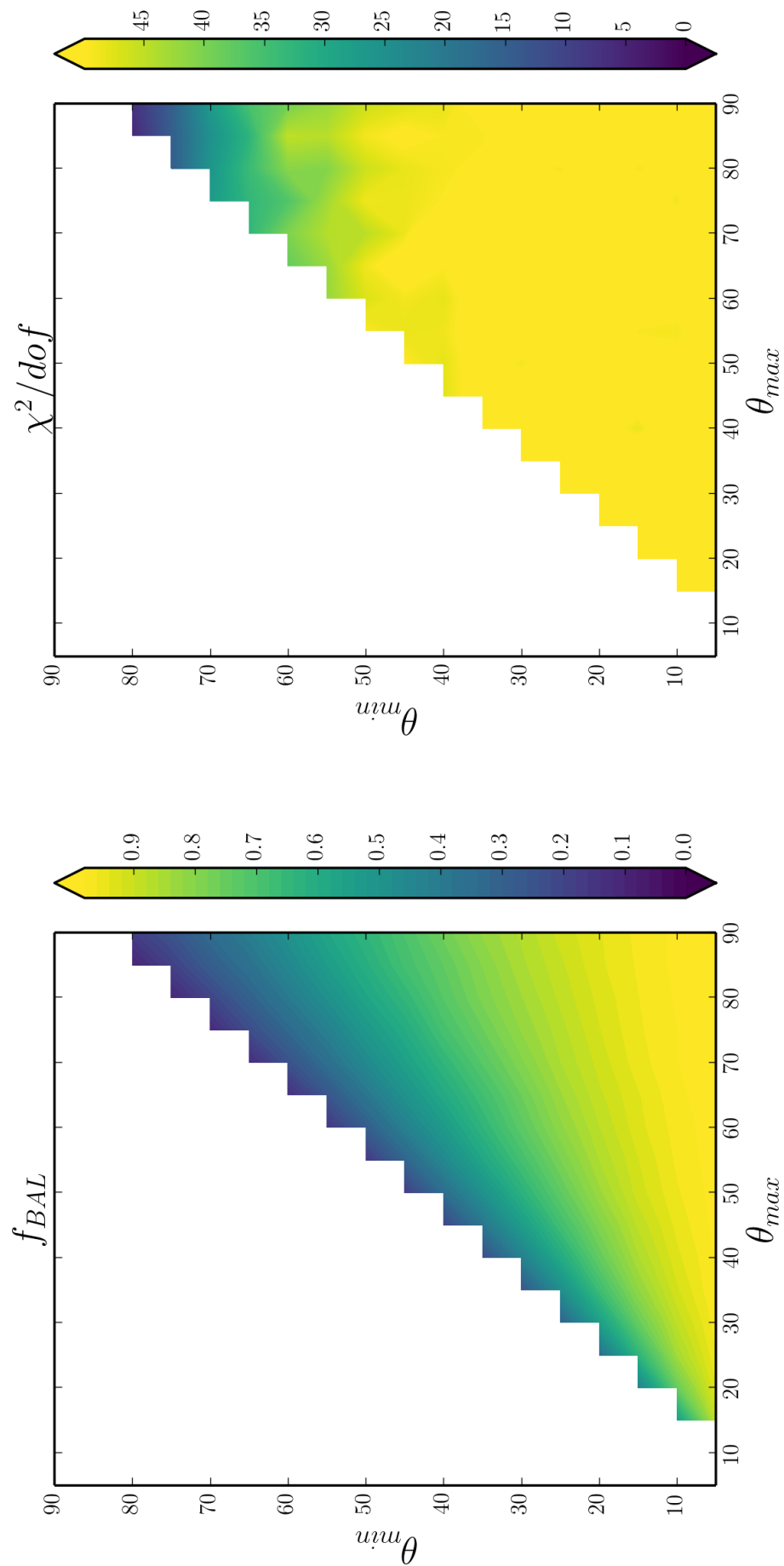


FIGURE 3.5: The geometry of the toy model used to carry out the Monte Carlo simulations

3. For each mock sample, a EW_0 is drawn from the intrinsic gaussian.
4. a mock EW is estimated such that $\text{EW} = \text{EW}_0/\epsilon(\theta)$, and this process is repeated to build up a mock sample of objects.
5. The number of objects in the mock sample with $\theta_{min} < \theta < \theta_{max}$ is recorded, providing an estimate of the expected BAL fraction for this wind geometry. This already includes a selection effect for the weaker continuum flux.
6. The value of the K-S test statistic is recorded, in which the mock BAL sample is compared to the real BAL sample. We also record the mean and variance of the mock sample. This allows us to ascertain which regions of parameter space best fit the observed BAL distribution

This process is repeated for a grid of θ_{min} and θ_{max} . The results are shown in figure 3.6, in which we plot the mean, standard deviation and f_{BAL} as a function of θ_{min} and θ_{max} . As expected, we find that equatorial viewing angles are strongly disfavoured.



3.4 Discussion

We have demonstrated that the EW distributions of the OIII emission line in quasars is not consistent with a model in which BALs are viewed from equatorial angles and the continuum emission originates from a foreshortened accretion disc. This conclusion would be strengthened were we to include limb darkening. This conclusion is extendible to the broad emission lines (IS IT?), with the caveat that those lines are dipole transitions and so opacity effects can change the angular distribution of emission. A number of other observations...

3.4.1 Radio Observations

Figure ? shows the equivalent width distributions in radio-loud quasars, split into core or lobe dominated. This designation is commonly used as an orientation indicator ([Orr & Browne 1982](#); [Wills & Brotherton 1995](#)). Although th

In this case, we can see that A full investigation of this is beyond the scope

3.4.2 Polarisation

Discuss polarisation

3.4.3 Compton-thick Fractions

Compton-thick Fractions

3.4.4 Theoretical Considerations

Discuss Proga models: They tend to rise fairly equatorially (see eg. PK04) Talk to Nick?

3.5 Conclusions

We find four possible scenarios:

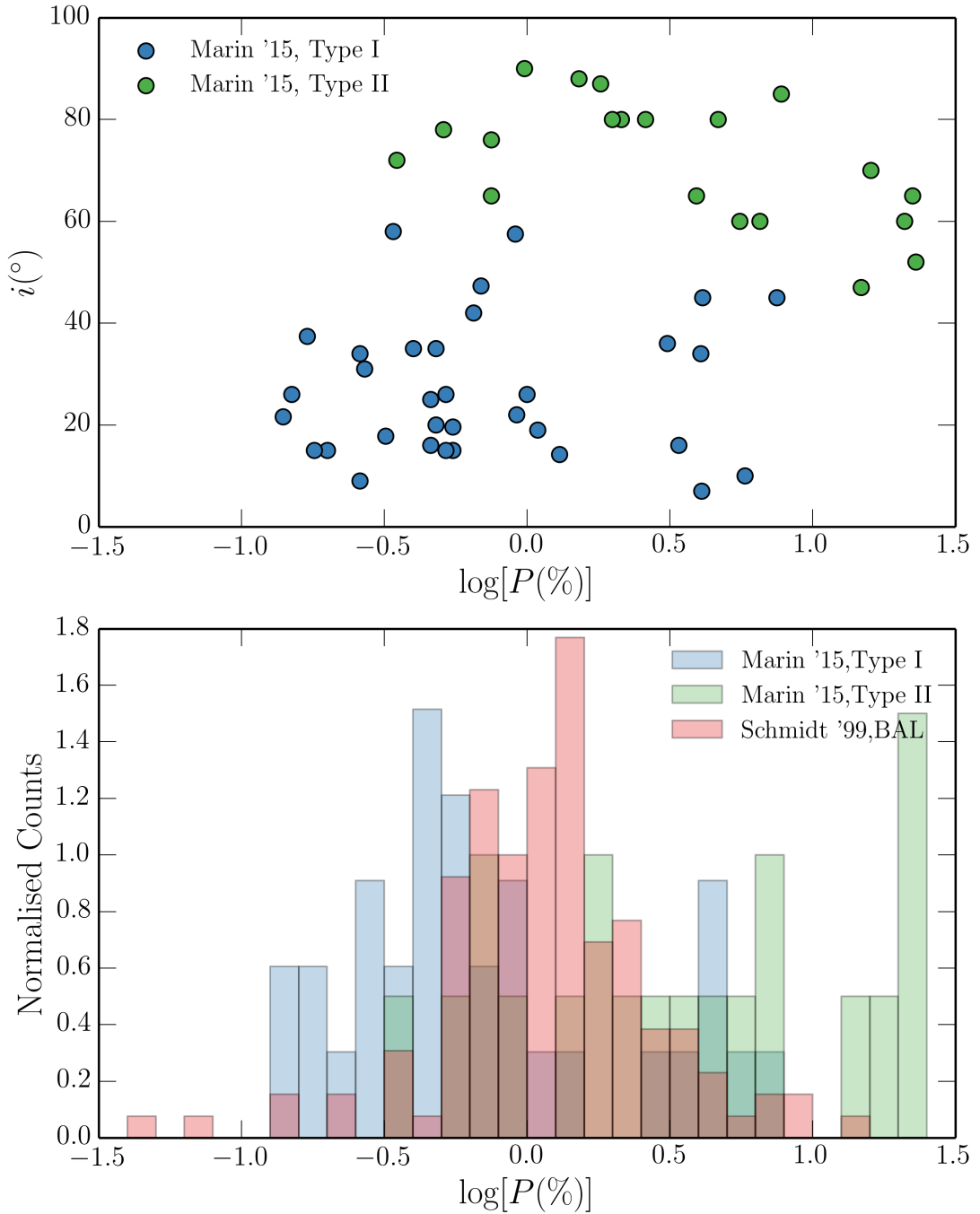


FIGURE 3.7: *Top:* Polarisation percentages as a function of measured inclination from Marin et al. (2015) for Type I and Type II AGN. *Bottom:* Histograms of polarisation percentages for BAL quasars from Schmidt et al. (1999) together with the Marin et al. (2015) AGN sample.

- *Scenario 1:* Quasar discs are much more isotropic than one might expect from an SS73 type disc. We have ascertained that general relativistic effects cannot account for discrepancy in the UV. Reprocessing by surrounding dense plasma with a large covering factor, or limb brightening caused by X-ray irradiation, may provide possible explanations which we do not yet confirm or refute.
- *Scenario 2:* Quasar discs are strongly anisotropic, as expected from a geometrically thin, optically thick accretion disc. In this case we expect $f_{BAL} \sim 1$ due to the selection effects at work, and a velocity field yadiyada.
- *Scenario 3:* BAL outflows are more collimated than expected from early polarisation measurements. This easily explains the emission line properties of BAL and non-BAL quasars. However, equatorial geometries have been most successful when modelling BAL quasars, and there are clear differences in the polarisation properties of BAL and non-BAL quasars. We recommend that future RT modelling efforts explore different outflow geometries and that detailed polarisation modelling is undertaken to constrain the outflow opening angles.
- *Scenario 4:* The geometric unification model does not explain the incidence of BALs in quasar, or requires an additional component which is *time-dependent*, such as an evolutionary or accretion state origin for BAL outflows. In this scenario, BAL quasars would be seen from very similar angles to non-BAL quasars. However, the evidence for this is limited and there is no good model for why outflows would exist only for $\sim 20\%$ of a quasar's lifetime. Even if this is the case, then the covering factor of the outflow still needs to be constrained in order to estimate the BAL duty cycle.

Of these, we favour scenario 3, as RT modelling of complex geometries is often degenerate (see Borguet et al. 2010 and Matthews et al. 2015 for details) and the differences in measured polarisation angle to not necessarily

Bibliography

- Alexander D. M., Bauer F. E., Brandt W. N., Daddi E., Hickox R. C., Lehmer B. D., Luo B., Xue Y. Q., Young M., Comastri A., Del Moro A., Fabian A. C., Gilli R., Goulding A. D., Mainieri V., Mullaney J. R., Paolillo M., Rafferty D. A., Schneider D. P., Shemmer O., Vignali C., 2011, ApJ 738, 44
- Allen J. T., Hewett P. C., Maddox N., Richards G. T., Belokurov V., 2011, MNRAS 410, 860
- Antonucci R., 1988, in M. Kafatos (ed.), Supermassive Black Holes, p. 26
- Antonucci R., 2013, Nature 495, 165
- Antonucci R., Geller R., Goodrich R. W., Miller J. S., 1996, ApJ 472, 502
- Antonucci R. R. J., Miller J. S., 1985, ApJ 297, 621
- Arévalo P., Uttley P., 2006, MNRAS 367, 801
- Balbus S. A., Hawley J. F., 1991, ApJ 376, 214
- Baldi R. D., Capetti A., Robinson A., Laor A., Behar E., 2016, MNRAS
- Baptista R., Silveira C., Steiner J. E., Horne K., 2000, MNRAS 314, 713
- Bartlett E., 2013, Ph.D. thesis, University of Southampton
- Begelman M. C., McKee C. F., Shields G. A., 1983, ApJ 271, 70
- Belloni T. (ed.), 2010, The Jet Paradigm, Vol. 794 of *Lecture Notes in Physics*, Berlin Springer Verlag
- Benz A. O., Fuerst E., Kiplinger A. L., 1983, Nature 302, 45
- Blandford R. D., Payne D. G., 1982, MNRAS 199, 883

- Blandford R. D., Znajek R. L., 1977, MNRAS 179, 433
- Bondi H., 1952, MNRAS 112, 195
- Bondi H., Hoyle F., 1944, MNRAS 104, 273
- Braito V., Reeves J. N., Dewangan G. C., George I., Griffiths R. E., Markowitz A., Nandra K., Porquet D., Ptak A., Turner T. J., Yaqoob T., Weaver K., 2007, ApJ 670, 978
- Capellupo D. M., Netzer H., Lira P., Trakhtenbrot B., Mejía-Restrepo J., 2015, MNRAS 446, 3427
- Cappi M., Mihara T., Matsuoka M., Hayashida K., Weaver K. A., Otani C., 1996, ApJ 458, 149
- Cassinelli J. P., 1979, ARAA 17, 275
- Chartas G., Kochanek C. S., Dai X., Poindexter S., Garmire G., 2009, ApJ 693, 174
- Cohen M. H., Ogle P. M., Tran H. D., Vermeulen R. C., Miller J. S., Goodrich R. W., Martel A. R., 1995, ApJ Letters 448, L77
- Cohen R. D., Puetter R. C., Rudy R. J., Ake T. B., Foltz C. B., 1986, ApJ 311, 135
- Connolly S. D., McHardy I. M., Dwelly T., 2014, MNRAS 440, 3503
- Coppejans D. L., Körding E. G., Miller-Jones J. C. A., Rupen M. P., Knigge C., Sivakoff G. R., Groot P. J., 2015, MNRAS 451, 3801
- Cordova F. A., Mason K. O., 1982, ApJ 260, 716
- Crenshaw D. M., Rodriguez-Pascual P. M., Penton S. V., Edelson R. A., Alloin D., Ayres T. R., Clavel J., Horne K., Johnson W. N., Kaspi S., Korista K. T., Kriss G. A., Krolik J. H., Malkan M. A., Maoz D., Netzer H., O'Brien P. T., Peterson B. M., Reichert G. A., Shull J. M., Ulrich M.-H., Wamsteker W., Warwick R. S., Yaqoob T., Balonek T. J., Barr P., Bromage G. E., Carini M., Carone T. E., Cheng F.-Z., Chuvaev K. K., Dietrich M., Doroshenko V. T., Dultzin-Hacyan D., Filippenko A. V., Gaskell C. M., Glass I. S., Goad M. R., Hutchings J., Kazanas D., Kollatschny W., Koratkar A. P., Laor A., Leighly K., Lyutyi V. M., MacAlpine G. M., Malkov Y. F., Martin P. G., McCollum B., Merkulova N. I., Metik L., Metlov V. G., Miller H. R., Morris S. L.,

- Oknyanskij V. L., Penfold J., Perez E., Perola G. C., Pike G., Pogge R. W., Pronik I., Pronik V. I., Ptak R. L., Recondo-Gonzalez M. C., Rodriguez-Espinoza J. M., Rokaki E. L., Roland J., Sadun A. C., Salamanca I., Santos-Lleo M., Sergeev S. G., Smith S. M., Snijders M. A. J., Sparke L. S., Stirpe G. M., Stoner R. E., Sun W.-H., van Groningen E., Wagner R. M., Wagner S., Wanders I., Welsh W. F., Weymann R. J., Wilkes B. J., Zheng W., 1996, ApJ 470, 322
- Dabrowski Y., Fabian A. C., Iwasawa K., Lasenby A. N., Reynolds C. S., 1997, MNRAS 288, L11
- Dai X., Shankar F., Sivakoff G. R., 2012, ApJ 757, 180
- Davis S. W., Hubeny I., 2006, ApJs 164, 530
- Davis S. W., Woo J.-H., Blaes O. M., 2007, ApJ 668, 682
- Denney K. D., De Rosa G., Croxall K., Gupta A., Bentz M. C., Fausnaugh M. M., Grier C. J., Martini P., Mathur S., Peterson B. M., Pogge R. W., Shappee B. J., 2014, ApJ 796, 134
- Dexter J., Agol E., 2011, ApJ Letters 727, L24
- Dhillon V. S., 1996, in A. Evans, J. H. Wood (eds.), IAU Colloq. 158: Cataclysmic Variables and Related Objects, Vol. 208 of *Astrophysics and Space Science Library*, 3
- Dhillon V. S., Rutten R. G. M., 1995, MNRAS 277, 777
- Díaz Trigo M., Boirin L., 2015, ArXiv e-prints
- Done C., Davis S. W., Jin C., Blaes O., Ward M., 2012, MNRAS 420, 1848
- Done C., Jin C., 2015, ArXiv e-prints
- Drew J., Verbunt F., 1985, MNRAS 213, 191
- Echevarria J., 1988, MNRAS 233, 513
- Edelson R., Gelbord J. M., Horne K., McHardy I. M., Peterson B. M., Arévalo P., Breeveld A. A., De Rosa G., Evans P. A., Goad M. R., Kriss G. A., Brandt W. N., Gehrels N., Grupe D., Kennea J. A., Kochanek C. S., Nousek J. A., Papadakis I., Siegel M., Starkey D., Uttley P., Vaughan S., Young S., Barth A. J., Bentz M. C.,

- Brewer B. J., Crenshaw D. M., Dalla Bontà E., De Lorenzo-Cáceres A., Denney K. D., Dietrich M., Ely J., Fausnaugh M. M., Grier C. J., Hall P. B., Kaastra J., Kelly B. C., Korista K. T., Lira P., Mathur S., Netzer H., Pancoast A., Pei L., Pogge R. W., Schimoia J. S., Treu T., Vestergaard M., Villforth C., Yan H., Zu Y., 2015, ApJ 806, 129
- Edge D. O., Shakeshaft J. R., McAdam W. B., Baldwin J. E., Archer S., 1959, MmRA 68, 37
- Eggleton P. P., 1983, ApJ 268, 368
- Ehman J. R., Dixon R. S., Kraus J. D., 1970, AJ 75, 351
- Ekers J. A., 1969, Australian Journal of Physics Astrophysical Supplement 7
- Elitzur M., 2012, ApJ Letters 747, L33
- Elitzur M., Ho L. C., Trump J. R., 2014, MNRAS 438, 3340
- Elvis M., 2000, ApJ 545, 63
- Elvis M., Wilkes B. J., McDowell J. C., Green R. F., Bechtold J., Willner S. P., Oey M. S., Polomski E., Cutri R., 1994, ApJs 95, 1
- Fabian A. C., 2012, ARAA 50, 455
- Fabian A. C., Kunieda H., Inoue S., Matsuoka M., Mihara T., Miyamoto S., Otani C., Ricker G., Tanaka Y., Yamauchi M., Yaqoob T., 1994, PASJ 46, L59
- Fabian A. C., Nandra K., Reynolds C. S., Brandt W. N., Otani C., Tanaka Y., Inoue H., Iwasawa K., 1995, MNRAS 277, L11
- Fath E. A., 1909, Lick Observatory Bulletin 5, 71
- Fender R. P., 2001, MNRAS 322, 31
- Fender R. P., Belloni T. M., Gallo E., 2004, MNRAS 355, 1105
- Fender R. P., Gallo E., Russell D., 2010, MNRAS 406, 1425
- Frank J., King A., Raine D., 1992, Accretion power in astrophysics.
- Gallo E., Fender R. P., Pooley G. G., 2003, MNRAS 344, 60

- Gandhi P., Hönig S. F., Kishimoto M., 2015, ApJ 812, 113
- Gandhi P., Terashima Y., Yamada S., Mushotzky R. F., Ueda Y., Baumgartner W. H., Alexander D. M., Malzac J., Vaghmare K., Takahashi T., Done C., 2013, ApJ 773, 51
- Ghosh K. K., Punsly B., 2007, ApJ Letters 661, L139
- Gierliński M., Done C., 2004, MNRAS 349, L7
- Gierliński M., Done C., 2006, MNRAS 371, L16
- Gofford J., Reeves J. N., Braito V., Nardini E., Costa M. T., Matzeu G. A., O'Brien P., Ward M., Turner T. J., Miller L., 2014, ApJ 784, 77
- Gofford J., Reeves J. N., McLaughlin D. E., Braito V., Turner T. J., Tombesi F., Cappi M., 2015, MNRAS 451, 4169
- Gofford J., Reeves J. N., Tombesi F., Braito V., Turner T. J., Miller L., Cappi M., 2013, MNRAS 430, 60
- Goodrich R. W., Miller J. S., 1995, ApJ Letters 448, L73
- Green A. R., McHardy I. M., Lehto H. J., 1993, MNRAS 265, 664
- Greenstein J. L., Oke J. B., 1982, ApJ 258, 209
- Groot P. J., Rutten R. G. M., van Paradijs J., 2004, A&A 417, 283
- Gültekin K., Richstone D. O., Gebhardt K., Lauer T. R., Tremaine S., Aller M. C., Bender R., Dressler A., Faber S. M., Filippenko A. V., Green R., Ho L. C., Kormendy J., Magorrian J., Pinkney J., Siopis C., 2009, ApJ 698, 198
- Haardt F., Maraschi L., 1991, ApJ Letters 380, L51
- Halpern J. P., 1984, ApJ 281, 90
- Häring N., Rix H.-W., 2004, ApJ Letters 604, L89
- Hassall B. J. M., 1985, MNRAS 216, 335
- Haug K., 1987, AP&SS 130, 91
- Hazard C., Mackey M. B., Shimmins A. J., 1963, Nature 197, 1037

- Heap S. R., Boggess A., Holm A., Klinglesmith D. A., Sparks W., West D., Wu C. C., Boksenberg A., Willis A., Wilson R., Macchetto F., Selvelli P. O., Stickland D., Greenstein J. L., Hutchings J. B., Underhill A. B., Viotti R., Whelan J. A. J., 1978, *Nature* 275, 385
- Heil L. M., Vaughan S., Uttley P., 2012, *MNRAS* 422, 2620
- Hessman F. V., Robinson E. L., Nather R. E., Zhang E.-H., 1984, *ApJ* 286, 747
- Higginbottom N., Knigge C., Long K. S., Sim S. A., Matthews J. H., 2013, *MNRAS* 436, 1390
- Hoare M. G., Drew J. E., 1991, *MNRAS* 249, 452
- Hoare M. G., Drew J. E., 1993, *MNRAS* 260, 647
- Hogg J. D., Reynolds C., 2015, ArXiv e-prints
- Honeycutt R. K., Schlegel E. M., Kaitchuck R. H., 1986, *ApJ* 302, 388
- Höning S. F., Kishimoto M., Tristram K. R. W., Prieto M. A., Gandhi P., Asmus D., Antonucci R., Burtscher L., Duschl W. J., Weigelt G., 2013, *ApJ* 771, 87
- Horne K., 1993, Eclipse Mapping of Accretion Disks: The First Decade, 117
- Horne K., Marsh T. R., 1986, *MNRAS* 218, 761
- Hoyle F., Lyttleton R. A., 1939, Proceedings of the Cambridge Philosophical Society 35, 405
- Hubeny I., Agol E., Blaes O., Krolik J. H., 2000, *ApJ* 533, 710
- Idan I., Lasota J.-P., Hameury J.-M., Shaviv G., 2010, *A&A* 519, A117
- Ioannou Z., van Zyl L., Naylor T., Charles P. A., Margon B., Koch-Miramond L., Illovaisky S., 2003, *A&A* 399, 211
- Iwasawa K., Fabian A. C., Mushotzky R. F., Brandt W. N., Awaki H., Kunieda H., 1996a, *MNRAS* 279, 837
- Iwasawa K., Fabian A. C., Reynolds C. S., Nandra K., Otani C., Inoue H., Hayashida K., Brandt W. N., Dotani T., Kunieda H., Matsuoka M., Tanaka Y., 1996b, *MNRAS* 282, 1038

- Janiuk A., Czerny B., Madejski G. M., 2001, ApJ 557, 408
- Kaastra J. S., Mewe R., Liedahl D. A., Komossa S., Brinkman A. C., 2000, A&A 354, L83
- Kaastra J. S., Paerels F. B. S., Durret F., Schindler S., Richter P., 2008, SSR 134, 155
- Kafka S., Honeycutt R. K., 2004, AJ 128, 2420
- King A., 2003, ApJ Letters 596, L27
- Knigge C., Baraffe I., Patterson J., 2011, ApJs 194, 28
- Knigge C., Drew J. E., 1997, ApJ 486, 445
- Knigge C., Long K. S., Blair W. P., Wade R. A., 1997, ApJ 476, 291
- Knigge C., Long K. S., Wade R. A., Baptista R., Horne K., Hubeny I., Rutten R. G. M., 1998a, ApJ 499, 414
- Knigge C., Long K. S., Wade R. A., Baptista R., Horne K., Hubeny I., Rutten R. G. M., 1998b, ApJ 499, 414
- Knigge C., Scaringi S., Goad M. R., Cottis C. E., 2008, MNRAS 386, 1426
- Koratkar A., Blaes O., 1999, PASP 111, 1
- Körding E., Rupen M., Knigge C., Fender R., Dhawan V., Templeton M., Muxlow T., 2008, Science 320, 1318
- Kotov O., Churazov E., Gilfanov M., 2001, MNRAS 327, 799
- Kraft R. P., Mathews J., Greenstein J. L., 1962, ApJ 136, 312
- Kriss G. A., Krolik J. H., Otani C., Espey B. R., Turner T. J., Kii T., Tsvetanov Z., Takahashi T., Davidsen A. F., Tashiro M., Zheng W., Murakami S., Petre R., Mihara T., 1996, ApJ 467, 629
- Krolik J. H., Begelman M. C., 1986, in Bulletin of the American Astronomical Society, Vol. 18 of *BAAS*, 903
- Kuulkers E., Motta S., Kajava J., Homan J., Fender R., Jonker P., 2015, The Astronomer's Telegram 7647

- La Dous C., 1989, MNRAS 238, 935
- Laor A., 1991, ApJ 376, 90
- Laor A., Davis S. W., 2014, MNRAS 438, 3024
- Lasota J.-P., 2001, NAR 45, 449
- Lazarova M. S., Canalizo G., Lacy M., Sajina A., 2012, ApJ 755, 29
- Liebert J., Stockman H. S., 1985, in D. Q. Lamb, J. Patterson (eds.), *Cataclysmic Variables and Low-Mass X-ray Binaries*, Vol. 113 of *Astrophysics and Space Science Library*, p. 151
- Long K. S., Blair W. P., Davidsen A. F., Bowers C. W., Dixon W. V. D., Durrance S. T., Feldman P. D., Henry R. C., Kriss G. A., Kruk J. W., Moos H. W., Vancura O., Ferguson H. C., Kimble R. A., 1991, ApJ Letters 381, L25
- Long K. S., Knigge C., 2002, ApJ 579, 725
- Long K. S., Wade R. A., Blair W. P., Davidsen A. F., Hubeny I., 1994, ApJ 426, 704
- Lusso E., Worseck G., Hennawi J. F., Prochaska J. X., Vignali C., Stern J., O'Meara J. M., 2015, MNRAS 449, 4204
- Lynden-Bell D., 1969, Nature 223, 690
- Lyubarskii Y. E., 1997, MNRAS 292, 679
- Madau P., Ghisellini G., Fabian A. C., 1994, MNRAS 270, L17
- Magdziarz P., Blaes O. M., Zdziarski A. A., Johnson W. N., Smith D. A., 1998, MNRAS 301, 179
- Mangham S. W., Knigge C., Matthews J. H., Long K. S., Sim S. A., Higginbottom N., 2016, in prep.
- Marinucci A., Bianchi S., Matt G., Alexander D. M., Baloković M., Bauer F. E., Brandt W. N., Gandhi P., Guainazzi M., Harrison F. A., Iwasawa K., Koss M., Madsen K. K., Nicastro F., Puccetti S., Ricci C., Stern D., Walton D. J., 2016, MNRAS 456, L94
- Marscher A. P., 2006, in P. A. Hughes, J. N. Bregman (eds.), *Relativistic Jets: The Common Physics of AGN, Microquasars, and Gamma-Ray Bursts*, Vol. 856 of *American Institute of Physics Conference Series*, p. 1

- Marsh T. R., Horne K., 1990, ApJ 349, 593
- Matt G., Guainazzi M., Maiolino R., 2003, MNRAS 342, 422
- Matzeu G. A., Reeves J. N., Nardini E., Braito V., Costa M. T., Tombesi F., Gofford J., 2016, MNRAS 458, 1311
- Mauche C. W., 1996, ArXiv Astrophysics e-prints
- Mauche C. W., Raymond J. C., 1987, ApJ 323, 690
- McConnell N. J., Ma C.-P., 2013, ApJ 764, 184
- McHardy I. M., Koerding E., Knigge C., Uttley P., Fender R. P., 2006, Nature 444, 730
- Mihalas D. M., 1982, Stellar atmospheres.
- Miller L., Turner T. J., 2013, ApJ Letters 773, L5
- Miller L., Turner T. J., Reeves J. N., 2008, A&A 483, 437
- Misra R., Kembhavi A. K., 1998, ApJ 499, 205
- Mitsuda K., Inoue H., Nakamura N., Tanaka Y., 1989, PASJ 41, 97
- Morgan C. W., Kochanek C. S., Morgan N. D., Falco E. E., 2010, ApJ 712, 1129
- Motta S., Beardmore A., Oates S., Sanna N. P. M. K. A., Kuulkers E., Kajava J., Sanchez-Fernandez C., 2015, The Astronomer's Telegram 7665
- Muñoz-Darias T., Coriat M., Plant D. S., Ponti G., Fender R. P., Dunn R. J. H., 2013, MNRAS 432, 1330
- Murray N., Chiang J., 1996, Nature 382, 789
- Murray N., Chiang J., 1997, ApJ 474, 91
- Murray N., Chiang J., Grossman S. A., Voit G. M., 1995, ApJ 451, 498
- Nandra K., Pounds K. A., 1994, MNRAS 268, 405
- Narayan R., McClintock J. E., 2012, MNRAS 419, L69
- Narayan R., McClintock J. E., Tchekhovskoy A., 2014, Energy Extraction from Spinning Black Holes Via Relativistic Jets, 523

- Narayan R., Yi I., 1994, ApJ Letters 428, L13
- Narayan R., Yi I., 1995, ApJ 452, 710
- Neugebauer G., Oke J. B., Becklin E. E., Matthews K., 1979, ApJ 230, 79
- Noebauer U. M., Long K. S., Sim S. A., Knigge C., 2010, ApJ 719, 1932
- Orr A., Molendi S., Fiore F., Grandi P., Parmar A. N., Owens A., 1997, A&A 324, L77
- Orr M. J. L., Browne I. W. A., 1982, MNRAS 200, 1067
- Osaki Y., 1974, PASJ 26, 429
- Otani C., Kii T., Reynolds C. S., Fabian A. C., Iwasawa K., Hayashida K., Inoue H., Kunieda H., Makino F., Matsuoka M., Tanaka Y., 1996, PASJ 48, 211
- Patterson J., 1984, ApJs 54, 443
- Patterson J., 1994, PASP 106, 209
- Patterson J., Patino R., Thorstensen J. R., Harvey D., Skillman D. R., Ringwald F. A., 1996, AJ 111, 2422
- Penrose R., Floyd R. M., 1971, Nature Physical Science 229, 177
- Perley R. A., Dreher J. W., Cowan J. J., 1984, ApJ Letters 285, L35
- Ponti G., Fender R. P., Begelman M. C., Dunn R. J. H., Neilsen J., Coriat M., 2012, MNRAS 422, L11
- Potash R. I., Wardle J. F. C., 1980, ApJ 239, 42
- Pounds K. A., Nandra K., Stewart G. C., Leighly K., 1989, MNRAS 240, 769
- Pounds K. A., Reeves J. N., 2009, MNRAS 397, 249
- Puccetti S., Fiore F., Risaliti G., Capalbi M., Elvis M., Nicastro F., 2007, MNRAS 377, 607
- Puebla R. E., Diaz M. P., Hillier D. J., Hubeny I., 2011, ApJ 736, 17
- Reeves J. N., O'Brien P. T., Ward M. J., 2003, ApJ Letters 593, L65

- Reynolds C. S., 1999, in J. Poutanen, R. Svensson (eds.), High Energy Processes in Accreting Black Holes, Vol. 161 of *Astronomical Society of the Pacific Conference Series*, 178
- Reynolds C. S., Fabian A. C., 1995, MNRAS 273, 1167
- Ringwald F. A., Naylor T., 1998, AJ 115, 286
- Risaliti G., Elvis M., Fabbiano G., Baldi A., Zezas A., Salvati M., 2007, ApJ Letters 659, L111
- Risaliti G., Elvis M., Nicastro F., 2002, ApJ 571, 234
- Ross R. R., Fabian A. C., 2005, MNRAS 358, 211
- Rottenberg J. A., 1952, MNRAS 112, 125
- Rutten R. G. M., van Paradijs J., Tinbergen J., 1992, A&A 260, 213
- Scaringi S., Körding E., Uttley P., Knigge C., Groot P. J., Still M., 2012, MNRAS 421, 2854
- Scaringi S., Maccarone T. J., Koerding E., Knigge C., Vaughan S., Marsh T. R., Aranzana E., Dhillon V., Barros S. C. C., 2015, ArXiv e-prints
- Schmidt M., 1963, Nature 197, 1040
- Schmidt M., 1965a, ApJ 141, 1295
- Schmidt M., 1965b, ApJ 141, 1
- Setti G., Woltjer L., 1989, A&A 224, L21
- Seyfert C. K., 1943, ApJ 97, 28
- Shakura N. I., Sunyaev R. A., 1973, A&A 24, 337
- Shaviv G., Wehrse R., 1991, A&A 251, 117
- Shi Y., Rieke G. H., Smith P., Rigby J., Hines D., Donley J., Schmidt G., Diamond-Stanic A. M., 2010, ApJ 714, 115
- Shlosman I., Vitello P., 1993, ApJ 409, 372
- Silk J., Rees M. J., 1998, A&A 331, L1

- Silva C., Uttley P., Costantini E., 2015, in The Extremes of Black Hole Accretion, 63
- Sim S. A., Long K. S., Miller L., Turner T. J., 2008, MNRAS 388, 611
- Sim S. A., Miller L., Long K. S., Turner T. J., Reeves J. N., 2010a, MNRAS 404, 1369
- Sim S. A., Proga D., Miller L., Long K. S., Turner T. J., 2010b, MNRAS 408, 1396
- Smak J., 1981, ACTAA 31, 395
- Springel V., Di Matteo T., Hernquist L., 2005, ApJ Letters 620, L79
- Stockman H. S., Angel J. R. P., Miley G. K., 1979, ApJ Letters 227, L55
- Struve O., 1935, ApJ 81, 66
- Suleimanov V., Hertfelder M., Werner K., Kley W., 2014, ArXiv e-prints
- Thorne K. S., 1974, ApJ 191, 507
- Tohline J. E., Osterbrock D. E., 1976, ApJ Letters 210, L117
- Tombesi F., Cappi M., Reeves J. N., Palumbo G. G. C., Yaqoob T., Braito V., Dadina M., 2010, A&A 521, A57
- Tombesi F., Meléndez M., Veilleux S., Reeves J. N., González-Alfonso E., Reynolds C. S., 2015, Nature 519, 436
- Tran H. D., 2001, ApJ Letters 554, L19
- Urrutia T., Becker R. H., White R. L., Glikman E., Lacy M., Hodge J., Gregg M. D., 2009, ApJ 698, 1095
- Urry C. M., Padovani P., 1995, PASP 107, 803
- Uttley P., Cackett E. M., Fabian A. C., Kara E., Wilkins D. R., 2014, AAPR 22, 72
- Uttley P., McHardy I. M., 2001, MNRAS 323, L26
- Uttley P., McHardy I. M., Vaughan S., 2005, MNRAS 359, 345
- Van de Sande M., Scaringi S., Knigge C., 2015, MNRAS 448, 2430
- Wade R. A., 1984, MNRAS 208, 381
- Wade R. A., 1988, ApJ 335, 394

- Wang B., Han Z., 2012, NAR 56, 122
- Warner B., 2003, Cataclysmic Variable Stars
- Weymann R. J., Morris S. L., Foltz C. B., Hewett P. C., 1991, ApJ 373, 23
- White N. E., Stella L., Parmar A. N., 1988, ApJ 324, 363
- Wills B. J., Brotherton M. S., 1995, ApJ Letters 448, L81
- Woltjer L., 1959, ApJ 130, 38
- Woods D. T., Klein R. I., Castor J. I., McKee C. F., Bell J. B., 1996, ApJ 461, 767
- Zakamska N. L., Strauss M. A., Krolik J. H., Collinge M. J., Hall P. B., Hao L., Heckman T. M., Ivezić Ž., Richards G. T., Schlegel D. J., Schneider D. P., Strateva I., Vanden Berk D. E., Anderson S. F., Brinkmann J., 2003, AJ 126, 2125
- Zanstra H., 1929, Publications of the Dominion Astrophysical Observatory Victoria 4, 209
- Zhang S. N., Cui W., Chen W., 1997, ApJ Letters 482, L155
- Zhou H., Wang T., Wang H., Wang J., Yuan W., Lu Y., 2006, ApJ 639, 716